NASA TECHNICAL MEMORANDUM

NASA TM - 75238

A COMPARISON OF PREDICTIONS OBTAINED FROM WIND TUNNEL TESTS AND THE RESULTS FROM CRUISING FLIGHT (AIRBUS AND CONCORDE)

J. Berger

Translation of "Comparison entre les prévisions des essais en soufflerie et les resultats de vol en croisiere (Airbus et Concorde)," AGARD CP no. 242, report no. 20, presented at Flight Mechanics Panel Specialists Meeting on Performance Prediction Methods, Paris, France, Oct. 11-13, 1977.

PP @20.1 @)20.50

NATIONAL AERONAUTICS AND SPACE ADMINISTRATION
WASHINGTON, D.C. 20546 AUGUST 1979

STANDARD TITLE PAGE

1. Report No. NASA TM - 75238	2. Government Accession No.	3. Recipient's Catalog No.
4. Title and Subtitle A COMPARISON OF PREDICTIONS OBTAINED FROM WIND TUNNEL TESTS AND THE RESULTS FROM CRUISING FLIGHT (AIRBUS AND CONCORDE)		5. Report Date August 1979 6. Performing Organization Code
7. Author(s) J. Berger Aerospatiale - France		8. Performing Organization Report No. 10. Work Unit No.
9. Performing Organization Name and Address Leo Kanner Associates Redwood City, California 94063		11. Contract or Grant No. NASw-3199 13. Type of Report and Period Covered Translation
12. Sponsoring Agency Name and Address National Aeronautics and Space Administration, Washington, D.C. 20546		14. Sponsoring Agency Code

15. Supplementary Notes Translation of "Comparison entre le prévisions des essais en soufflerie et les resultats de vol en croisiere (Airbus et Concorde)," AGARD CP nº 242, exposé nº 20, presented at Flight Mechanics Panel Specialists Meeting on Performance Prediction Methods, Paris, France, Oct. 11-13, 1977. pp 20-1 - 20-50

16. Abstract

This report is the report given to the Agard Conference in June 1975 by the Aerospatiale engineers and deals with the cruising performance aspects of Airbus and Concorde.

Following a summary of the methods used to establish aerodynamic data and propulsion data (wind tunnel tests, bench tests, etc), we are making a comparison in the form of the drag (or thrust) difference between flight results and predictions made on the basis of these data.

Although certain hypothesis and improvements on aerodynamic data can be presented in order to explain the slight deficit found on Airbus and Concorde, we still must verify the characteristics of raw thrust, air flow and consumption of the gas generator-exhaust nozzle group, which are involved in the propulsion data.

17. Key Words (Selected by Author(s))	18. Distribution Statement
	Unclassified-Unlimited

19. Security Classif. (of this report)	20. Security Classif. (of this page)	21. No. of Pages	22. Price
Unclassified	Unclassified	71	

A COMPARISON OF PREDICTIONS OBTAINED FROM WIND TUNNEL TESTS AND THE RESULTS FROM CRUISING FLIGHT (AIRBUS AND CONCORDE)

J. Berger
(Aerospatiale - France)

1 - Introduction

This report follows one presented in June, 1975, at the /20-2* Agard Conference (conference proceedings no. 187, contribution no. 23) by AEROSPATIALE 1 .

It concerns the following:

- the Airbus, designed and developed by the European companies Hawker Siddeley Aviation, Deutsche Airbus, Aerospatiale and Airbus Industrie,
- the Concorde, designed and developed by the European companies Rolls Royce, Société Nationale d'Etude et de Construction de Moteur d'Avion, British Aircraft Corporation and Aérospatiale.

By limiting itself exclusively to cruising flight ($0.78 \leqslant M \leqslant 0.82$ for Airbus and M - 2.0 for Concorde), the report's objective is to present the methods employed to evaluate performances based on wind tunnel tests and test bench and then to compare them to results obtained in flight.

We are not trying here to find a solution to the eternal problem of distinguishing between drag and thrust by means of in-flight testing. The comparisons which will be made between predictions and flight results will be presented in the form of differences in external stresses applied to the plane (Δ Cx ext), in other words, the combination of aerodynamic stresses (coefficient A) and the propulsion stress (coefficient π).

---

* Numbers in the margin indicate pagination in the foreign text.

After a summary of certain definitions, we will explain /20-3 how aerodynamic and propulsion data for Airbus and Concorde have been evaluated, specifying clearly the content of each.

We will then give a summary of the features of in-flight testing equipment for the two planes, limiting ourselves to the parameters necessary for the calculation of performances.

Finally, we will present the results of the analysis carried out on the basis of the in-flight tests, without going into detail regarding the gas generator-exhaust nozzle group.

This flight-prediction comparison is to be regarded as a technical study. It does not concern itself with warranties made to buyers of these planes.

2 - Cruising Performance - Summary of Certain Definitions - Accuracy of Results

2.1 - Cruising Equilibrium Equations

Fig. 1 shows the planes equilibrium at zero side-slip and makes evident what from now on will be known as "aerodynamic data" corresponding to aerodynamic stresses, and "propulsion data" corresponding to propulsion stresses.

Fig. 2 places the preceding equations in the plane of the classical polar curve C_{XA}, C_{ZA}, by showing the differences between cruising at constant altitude and cruising at constant engine speed and the consequences which external stress variation can have on the operating point.

2.2 - Influence of External Stress Variation in Cruising on Plane's Fuel Consumption

Fig. 3 shows the influence of a decrease in external stresses

equivalent to a 1% increase in drag at a given lift.

This table based on fixed cruising speed and distance from destination, confirms well-known conclusions, namely;
- that a supersonic plane such as Concorde is more sensitive to external stress variations than a subsonic plane; this is in part due to the fact that it flies at constant speed;
- that, when designing a plane, it is always wise to make an allowance for maximal take-off mass and maximal tank capacity.

3 - Propulsion Data

These data are of a different nature whether we are talking about Airbus or Concorde. This subject has already been discussed at previous Agard conferences [2, 3] for Concorde .

3.1 - Airbus

The two Airbus engines are CF6 50 C made by General Electric; double flux engine.

In cruising, the bypass ratio is about 4.5 and the outlet expansion ratios are respectively on the order of 2.4 and 2.1 for the fan and the central engine.

The total air flow at M = 0.8 31,000 ft. is about 650 lb/s.

Data relating to the flange-to-flange engine-exhaust nozzle combination have been directly supplied by the motor mechanic in the form of a data sheet which can supply, for various total temperature and total pressure inlet conditions, the values of:
- air flow $W_1 = W_T$
- raw thrust $F_{G\,\pi}$
- consumption C

as a function of fan speed (N1), and all this for the isolated nacelle without external flow.

Raw thrust $F_{G\pi}$ is the sum, with the exclusion of everything else, of:

- the raw thrusts of fan (cold) and engine (hot) outlet,
- the friction and pressure drags of strut and cowl surfaces touched by the fan jet;
- friction and surface drag of central body surfaces touched by the fan jet.

Fig. 4 shows how this data sheet has been obtained. We will only summarize the main steps.

3.1.1 - Ground Bench Tests on a Scale 1 Engine Equipped with Exhaust Nozzle and Strut Section (Fig. 4a)

Based on these measurements, carried out with a "calibrated air intake duct", we can observe, for different reduced speeds $N_1/\sqrt{T_{t_1}}$, the following values necessary for cruising:

- ratio of total exhaust pressures : $\frac{PtJF}{Pt_1}$, $\frac{PtJm}{Pt_1}$ /20-4
- ratio of total temperature : $\frac{TtJm}{Tt_1}$
- reduced air flow : $\frac{W_1\sqrt{T_{t_1}}}{Pt_1}$
- reduced oil flow : $\frac{C}{Pt_1\sqrt{T_{t_1}}}$

All these values are valid for total pressure Pt_1 (of calibrated duct), total temperature Tt_1, normal static pressure Ps_∞ of ground bench fueling conditions, in other words different from cruising flight conditions.

These tests serve, therefore, to specify the internal features of the propulsion system, but cannot directly justify cruising thrusts. The components of cruising sonic outlet cannot be represented at fixed point.

3.1.2 - Transposition to Cruising Conditions

3.1.2.1 - Internal Features

Semi-empirical methods have been employed to transpose the preceding $N_1/\sqrt{T_{t_1}}$ functions

$$\frac{PT_{JF}}{Pt_1}\ ,\quad \frac{PT_{Jm}}{Pt_1}\ ,\quad \frac{T_{TJm}}{T_{T_1}}\ ,\quad \frac{W_1\sqrt{Tt_1}}{Pt_1}\ ,\quad \frac{C}{Pt_1\sqrt{T_{t_1}}}$$

of ground bench Pt_1, Tt_1 values to the Pt_1, Tt_1 values of cruising operations.

These transpostions are generally controlled and even re-adjusted by in-flight tests.

3.1.2.2 - Determination of Raw Thrust in Cruising

This is made by weighing models of the exhaust nozzle (1/10 scale approximately) geometrically similar to cruising shapes and with strut section (Fig. 4b).

From these measurements, carried out without external flow and with expansion ratios $\frac{PTJF}{P_{s\infty}}$, $\frac{PTJm}{P_{s\infty}}$ and temperatures Tt_{Jm} representative of cruising conditions, we obtain:

- raw thrust without friction FG, resulting from the corrected balance stress, stray stresses due to assembly and strut friction, cowl and central body stresses calculated for test conditions;
- nozzle thrust coefficients C_{JF} and C_{JM} compatible with FG.

The total of these results including friction drag in flight conditions of strut and cowl surfaces touched by the fan jet and of the central body touched by the fan jet makes it possible to compile a data sheet (engine - exhaust nozzle) which supplies the values

of W_1, FG_π , and C as a function of Pt_1, Tt_1, ps_∞ , $N_1/\sqrt{Tt_1}$.

By means of semi-empirical calculations, this booklet can take into account air and power collections.

3.1.3 - Air Intake

Tests carried out on a model (Fig. 5) and checked by in-flight tests make it possible to know the performance $\eta_1 = \frac{Pt_1}{Pt_\infty}$ at the compressor intake as a function of the Mach number of the plane.

This performance is independent of air flow in cruising.

3.1.4 - Summary of Propulsion Data

Fig. 6 illustrates the procedure followed. For given flight conditions and speed, we can obtain the values for raw thrust FG_π , catchment drag FD_π , air intake flow coefficient ε T and consumption C valid without external flow.

The influence of the external flow and of the wing unit on the raw thrust FG_π values will be taken into account in the aerodynamic data.

3.2 - Concorde /20-5

The four Concorde engines are Olympus made by Rolls Royce and SNECMA. They are simple flux, double body (BP and HP) with cruising expansion ratio at M = 2.0 on the order of 14.

Air flow in cruising at M = 2.0 55,000 ft. is about 210 lb/s.

Fig. 7 shows the components of the propulsion system of such

a plane.

3.2.1 - Gas Generator (Fig. 8)

Its intake is the compressor BP, its exhaust the sonic nozzle of the primary nozzle.

Altitude bench tests of a scale 1 engine placed downstream of an air intake duct simulating flight values of total pressure Pt_1, total temperature Tt_1 and static pressure $p_{s\infty}$ make it possible to compile a sheet supplying the values of

$$\frac{WJm\ \sqrt{Tt}_{Jm}}{K_C\ Pt_{Jm}} \quad ; \quad \frac{WJm\ \sqrt{Tt}_{Jm}}{K_C\ Ps_\infty} \quad , \quad \frac{Tt_{Jm}}{Tt_1}$$

(representing the features of the jet at the sonic nozzle of the variable section of the primary nozzle) and

$$W1\ \frac{\sqrt{Tt}_1}{Pt_1} \quad , \quad \frac{C}{Pt_1\ \sqrt{Tt}_1}$$

as a function of Pt_1, Tt_1, Ps_∞, $N1/\sqrt{Tt}_1$ and $N2/\sqrt{Tt}_1$.

3.2.2 - Air Intake (Fig. 9)

A 1/15 scale model of the two joint air intakes placed under the wing unit was tested according to the Mach number for cruising (the number of Reynolds is about ¼ that of flight, the boundary limit trap of the wing unit has been thickened so that the portion of boundary limit found in the wind tunnel is the same as that in flight).

From these tests we have been able to compile the data sheet with information regarding air intake and supplying the values of η_1 and ε_T as a function of α, M_∞, δ_2, η_B, ε_B.

3.2.3 - Exhaust Nozzle

This nozzle is of the convergent-divergent double flux type with secondary air injection at right angles with the sonic nozzle of the primary nozzle.

Raw thrust is defined as the difference obtained with external flow between, on the one hand, the total of internal and external stresses applied to real forms and in flight jet conditions and, on the other hand, the external stresses applied to an external reference form identical to that of aerodynamic plane models.

Two 1/20 scale models have been employed (with a plate simulating the symmetrical nozzle in order to recreate the plane's configuration) (see Fig. 10a for reference form and Fig. 10b for real form). Tests were carried out in cold gas (wind tunnel temperature).

Internal performances of the real form were readjusted based on tests carried out without external flow on a 1/10 scale model.

A theoretically determined hot gas correction was necessary. It affects raw thrust and the nozzle pressure characteristic (this was established in ref. 4).

These tests and corrections make it possible to compile a nozzle data sheet supplying the values for $F_G \pi$ and $\frac{Pt_s}{Pt_{sm}}$ as a function of

$M\infty$, $\frac{W_{jm}\sqrt{Tt_{Jm}}}{Kc\ Pt_{Jm}}$, $\frac{W_{Jm}\sqrt{Tt_{Jm}}}{Kc\ Ps_\infty}$ and $M = \frac{Ws\sqrt{Tt_s}}{W_{Jm}\sqrt{Tt_{Jm}}}$

3.2.4 - Secondary Flow

A 1/2 scale model representing with precision all uneven

features of the secondary duct was tested.

These tests have made it possible to compile a data sheet for secondary air which supplies the value of $\frac{PtS}{PtB}$ as a function of $\frac{WB\sqrt{Tt}^{1}}{PtB}$.

3.2.5 - Various Corrections

Heating of secondary flow: Air taken from the WHE air intake upstream of the compressor BP and considered in the air intake data sheet is heated during the cooling process of air-conditioning air which is taken directly by means of the compressor. It is reinjected in the secondary air at the intake of the exhaust nozzle. On the other hand, the secondary flow participates in the cooling of the engine crank case and its accessories. /20-6

Secondary duct bleeds: The nacelles are not perfectly tight. Ground tests have made it possible to estimate the bleed section equivalent to 1/2 nacelle (Fig. 12). The calculations take this into account assuming that all the catchment drag of this air is lost.

Primary duct bleed toward secondary duct: downstream of the outlet of the turbine BP. This air at temperature Ttjm is part of the secondary air supply process for the nozzle.

Condition of internal surface of secondary nozzle: The 1/20 scale models described in Chap. 3.2.3 are smoother than the plane though they have some moving obstructions. A stray drag must, therefore, be deducted from the raw thrust supplied by the nozzle data sheet.

3.2.6 - Recapitulation of Propulsion Data

Fig. 13 shows the procedure to be followed.

We can so obtain, for given flight conditions and a given regime N_1 and N_2 (or C), the values of raw thrust $F_{G\pi}$, of catchment drag $F_{D\pi}$, of the air intake flow coefficient ε_T and consumption C (or N_2).

4 - Aerodynamic Data

In this context it is also necessary to distinguish between Airbus and Concorde.

Fig. 14 shows the outline followed in order to go from the wind tunnel results obtained on the model to the final aerodynamic data representative of the plane in flight.

The subject has already been discussed at previous Agard conferences (2,3 for Concorde).

4.1 - Airbus

4.1.1 - Basic Model

Fig. 15 shows the assembly on a rod Z of the 1/38 scale model supposed to simulate the general shape of the plane in flight. The tests were carried out by setting out the boundary layer transition by means of silicon carbide grains as well as by leaving unaltered the boundary limit of the wing unit.

The model is equipped with:
- a smooth wing unit which allows several horizontal tail unit angles as well as rudder angles (δ_q);

- permeable pods with correct external fan cowl and engine cowl shapes.

These tests make it possible to obtain the values of C_{XB}, C_{ZB}, C_{mB}, as a function of M_∞, α, δ_{EM} and δq.

To simplify the explanation we have not mentioned the sideslip and elevator and rudder angles for which measurements have been taken.

The flights we are going to examine were made with almost null values for these parameters. Their slight influence was nevertheless taken into account in the analysis.

4.1.2 -Transposition to Flight Conditions

4.1.2.1 - Shape Correction Due to Wind Tunnel Assembly

Fig. 16 diagrams the assembly used with the 1/38 scale model. It makes it possible to estimate corrections ΔCx_{AR}, ΔCz_{AR} and ΔCm_{AR} due to assembly as a function of $M\infty$ and α.

4.1.2.2 - Friction Correction

Based on the wind tunnel test, on a flight at M = 0.8 30,000 ft., the mean Reynolds number goes from 2.5×10^6 to 47.5×10^6 for the wing unit and from 20×10^6 to 380×10^6 for the fuselage. This is the so-called Prandlt Schlichting applicable to the plate which has been employed.

Fig. 17 shows the transition line obtained from wing unit tests without setting off the boundary limit and displayed by means of acenaphtene sublimation.

Actually, tests where the transition has been set off are the ones generally used. On the other hand, with this correction, it is necessary to take into consideration the fact that the friction drag of external surfaces touched by the fan jet has been considered in the propulsion data.

4.1.2.3 - Motorization Correction /20-7

These corrections are described in detail in ref. 5, 6 . Here we will only summarize them.

The corrections are shown in Fig. 18. They can be divided into three groups.

a) Internal stress correction (Fig. 18a)

By scanning fan and central engine outlets, we can deduce, for the basic model:

- the raw thrust of the outlet of the fan and of the engine X_1 (Fo + Co),
- the inlet flow W_{10} from which we can deduce the corresponding catchment drag and the basic flow coefficient ε_{Ref}.

We can deduce the internal stress corrections on drag ($\Delta C_{X\ int}$) on lift ($\Delta C_{Z\ int}$) and the pitch momentum ($\Delta C_{m\ int}$) as a function of M_∞ and α .

b) Additive stress correction (Fig. 18a)

The coefficient ε_{Ref} is inferior to the in-flight coefficient ε_T.

To obtain this correction due to the difference ($\varepsilon_T - \varepsilon_{Ref}$), the basic model is equipped with the correct pod as far as the air intake is concerned up to the midship frame but deformed in the back. The addition of internal grills makes it possible to vary the flow according to values greater and smaller

than ε_{Ref}. The measurements are identical to the preceding ones for internal stress correction.

We can obtain the additive stress correction on drag ($\Delta C_{X\ ad}$), lift ($\Delta C_{Z\ ad}$) and pitch momentum ($\Delta C_{m\ ad}$) as a function of ($\varepsilon_T - \varepsilon_{Ref}$), M_∞ and α.

c) Pressure stress correction (Fig. 18b)

This correction is made necessary by the fact that the propulsion data are valid in the absence of external flow and with isolated nacelle and that the basic model has been tested with pods operating at natural flow. The correction is obtained by using pressure integrations on the wing unit, the strut, the fan cowl and engine cowl of a 1/19 scale model with motorized nacelle mounted on a demi-wing, which can simulate the following exhaust configurations:

1) Natural flow jet of basic model; tests carried out at $M\infty$. It gives pressure stresses on the wing unit, the strut, the fan cowl and engine cowl X_o (V + M + F + C);

2) correct cruising jet (expansion ratio and real temperature); tests carried out at $M_\infty = 0$ and identical to propulsion data. This gives the pressure stresses on the engine cowl and strut

$$[X_2\ (C + M)]\ M\infty = 0$$

3) Correct cruising jet (expansion ratio and real temperature); tests carried out at $M\infty$. This gives the pressure stresses on the wing unit, the strut, the fan cowl and engine cowl

$$[X_2\ (V + M + F + C)]M\infty$$

The combination of these three tests makes it possible to deter-

mine the pressure stress correction on the drag ($\Delta C_{X\ jet}$), on the lift ($\Delta C_{Z\ jet}$) and on pitch momentum ($\Delta C_{m\ jet}$) as a function of M_∞ and α .

4.1.2.4 - Stray drag

This correction takes into account all uneven features (condition of the surface, aerials, joints, additional air intakes, flow of air conditioning, etc) which could not be simulated on the wind tunnel model. It is the result of calculations based on the usual semi-empirical methods.

4.1.3 Recapitulation

Fig. 19 shows quantitatively the values relative to the various correction made on the basic model in order to obtain an equilibrated polar curve for Airbus cruising at M = 0.8 30,000 ft. ISA and 25 % alignment.

All these corrections represent about 21% of the plane's /20-8 drag. The most important factor is the friction correction (27%).

The fact that results are taken without setting off the boundary layer on the wing unit will be explained later.

4.2 - Concorde

4.2.1 - Basic Model

Fig. 20 diagrams the assembly on a rod of a 1/45 scale model which should represent the general forms of the plane in flight. We will later see that actually two shapes have been tested. The tests were carried out without artificial setting off of the transition. Visual display by means of naphtalene sublimation has

shown that, under test conditions, the flow was completely turbulent.

The model is equipped with:

- a wing unit with capacity for different elevator and rudder angles;
- permeable pods with separation stem for adjacent air intakes, first ramp and wing unit boundary layer trap. The back section of the pod has been distorted; it has a base and a sonic outlet which makes the air intake operate at supercritical regime. It is completely identical to the reference form described in chap. 3.2.3.

These tests make it possible to obtain the values of C_{XB}, C_{ZB} and C_{mB} as a function of M_∞ , α , δ_q .

As with Airbus, the influence of side-slip, rudder and elevator angles is not considered here, although the measurements have been taken. The flights which are going to be examined were carried out with almost null values for these parameters, the influence of which was, nevertheless, taken into consideration in the analysis.

4.2.2 - Transposition to Flight Conditions

4.2.2.1 - Shape Correction Due to Assembly in Wind Tunnel

Fig. 21 diagrams the assembly used on a 1/45 scale model. Pre-testing pressure measurements on the back section have demonstrated that the presence of lateral struts has no influence.
The assembly makes it possible to estimate the corrections $\Delta C_{X\,AR}$, $\Delta C_{Z\,AR}$, and $\Delta C_{m\,AR}$ as a function of M_∞ , and α .

4.2.2.2 - Friction Correction

Based on wind tunnel tests in flight at M = 2.0 55,000 ft., Reynolds number goes from $41 \cdot 10^6$ to $130 \cdot 10^6$ for the wing unit and from $91 \cdot 10^6$ to $288 \cdot 10^6$ for the fuselage. It is the so called Michel formula, applicable to the employed plate.

To take into account the non-athermanous temperature of the surfaces of the wing unit in flight, an artificial correction was considered.

4.2.2.3 - Motorization Corrections

These are shown in Fig. 22 and can be divided into two groups.

a) Internal stress and base stress correction.
This correction is obtained by the following procedure:
- probing of the sonic outlet to find out the values of exhaust Mach number (Me) which, together with the flow value, will make possible the calculation of the raw outlet thrust (X_{10});
- measurement of nacelle flow (WT) by flowmeter placed downstream of the nacelle (under these conditions weighing is not possible), which allows us to find out the basic flow coefficient ε_{Ref} and the catchment drag.
- usual weighing without flowmeter and measurement of base pressure which, by integration, make it possible to obtain the base stress.

Based on these tests we can estimate the internal drag correction and the base correction on the drag ($\Delta C_{X\ int}$ and $\Delta C_{X\ base}$), on the lift ($\Delta C_{Z\ int}$ and $\Delta C_{Z\ base}$) and on pitch momentum ($\Delta C_{m\ int}$ and $\Delta C_{m\ base}$) as well as the value of ε_{Ref} as a function of M_∞ and α .

b) Additive stress correction.

Based on the internal geometry of the model's nacelle, the value of ε_{Ref} is a maximum. To obtain the corrections due to flow reduction by variation of the 2nd pipe angle δ_2, the basic model has been equipped with pods identical to the basic ones but with a capacity for different δ_2 (as in flight, internal air intakes have a δ_2 greater by $0^{\circ},5$ than that of external intakes). /20-9

The sonic outlet has been adjusted for each of these values so that the air intakes remain supercritical.

The measurements are analogous to the preceding ones relating to internal drag and base drag corrections. Based on the differences resulting from measurements carried out at ε_{Ref}, we obtain the additive stress correction on drag ($\Delta C_{X\ ad}$), on the lift ($\Delta C_{Z\ ad}$) and on the pitch momentum ($\Delta C_{m\ ad}$) determined by δ_2 variation but presented as a function of ($\varepsilon_T - \varepsilon_{Ref}$), M_∞ and α .

4.2.2.4 - Stray Drag

This correction takes into account all uneven features (surface condition, aerials, additional air intakes, flow of air conditioning, etc.) which could not be simulated on the wind tunnel model.

Methods employed for evaluation are discussed in Ref. 3.

4.2.3 - Recapitulation

Fig. 23 shows quantitatively the values relative to the various corrections made on the basic model in order to obtain a polar curve for a pre-production 02 Concorde in cruising flight at M = 2.0 55,000 ft, ISA + 5, $\delta q = 0^{\circ},5$.

4.3 - General Comments on the Precision of Aerodynamic Data

It is very difficult to discuss this subject. Some authors (8) calculate that in transonic and supersonic wind tunnels, the C_X cannot be evaluated with better precision than Δ 100 C_X ± 0.05 which corresponds to ± 2% of the drag for Airbus and ± 3% for Concorde.

The data we are presenting are the result of:
- one series of tests with Airbus during which one polar curve based on Mach's number was measured;
- two series of tests with Concorde during which ten polar curves, were measured each time.

Under these conditions, it seems reasonable to state that the aerodynamic data are known with a precision of at least:

$$\Delta 100\ C_{X\ A}\ \underline{S}\ \pm 0.05 \text{ for Airbus}$$
with ± 2% of the drag

$$\Delta 100\ C_{X\ A}\ \underline{S}\ \pm 0.012 \text{ for Concorde}$$
with ± 0.7% of the drag

5 - Equipment for In Flight Testing

It is not our intention to describe in detail the in flight testing equipment for Airbus and Concorde. As far as the latter is concerned, such data is available in Ref. 7.

We will limit ourselves to an outline summary showing what has been used in the study of cruising performances.

5.1 - Airbus

Fig. 24 shows the parameters recorded on pre-production planes, the results of which were used in the study.

We can observe that the anemometric station has been adjusted as described in Ref. 7, in other words by kinetheodolite at low altitude and radar at high altitude. We have not mentioned internal engine test equipment. Let's just say that it is sufficient to control the various internal pressure and temperature parameters in the engine, though it cannot control the nozzle thrust coefficients.

5.2 - Concorde /20-10

Fig. 25 shows the parameters recorded on the pre-production 02 plane, the results of which were used in the study.

Comment:

- the nose-piece-receiver combination was adjusted as described in Ref 7, in other words by kinetheodolite at low altitude and radar at high altitude;
- the instantaneous mass is the average of 4 values obtained by means of gauges and flowmeter integration and based on measurements taken at take-off and landing;
- the mass flowmeters were adjusted individually on the engine during bench tests by using fuel at different temperatures.

Fig. 26 shows the parameters which were measured to follow the air intake and secondary flow. Other parameters, which are not mentioned here, control the internal characteristics of the gas generator and the exhaust nozzle.

6 - Flight Results - Comparisons with Predictions Based on Wind Tunnel Tests

As we have already mentioned, the results are presented in the

$\Delta C_{X\ ext}$ form, representing the difference in aerodynamic and propulsion stresses applied to the plane at in flight $C_{Z\ meas}$ and calculated according to the general formula described in Fig. 27, between in flight tests and predictions.

The datum lines are the "wind" lines. An increase in drag or a decrease in thrust correspond to a positive $\Delta C_{X\ ext}$.

We have only taken into consideration levels with a duration of about two minutes or flight parameters (regime, altitude, Mach, temperature, etc) which have been stabilized. The side-slip and warping angles never exceed $0^{o}.5$; their influence has, nevertheless, been taken into account.

Although a general diagram can be applied to both Airbus and Concorde, application details are not identical at all.

6.1 - Airbus

6.1.1 - In Flight Measurements

Based on the general outline described in Fig. 27, the following details must be evaluated:

- parameter of propulsion behavior: N_1 measured;
- propulsion data: average value for engine - exhaust nozzle group;
- plane geometry: CG calculated;
- nz: cosine of trajectory angle with horizontal. The variation of g with altitude and speed has been overlooked. This results in a maximum overestimation of the predicted C_x of Δ 100 C_X = 0.005.
- nx: calculated on the basis of information given by the anemometric station.

Under these conditions, by using the in flight measurement precisions mentioned in Fig. 24, we can estimate the precision of

independent parameters and infer the precision of $C_{X\ meas}$, C_X and, therefore, $\Delta\ C_{X\ ext}$.

The precision of the C_Z measurement is transformed into C_X precision by intervention of induced drag.

Without taking into account the precision of propulsion data or the dispersion between engines and planes, but considering the precision of aerodynamic data, we arrive to a precision for 100 $C_{X\ meas}$ on the order of $\pm$ 0.06.

6.1.2 - Results

The results presented here originate from 103 stabilized levels on 5 planes between 25,000 and 36,000 ft. at Mach's numbers near 0.78, 0.80 and 0.82.

Each flight $C_{X\ meas}$ was corrected by means of aerodynamic data in order to conform to the following conditions:

M = o.78 or 0.80 or 0.82
(the correction is always such that
Δ M $\leqslant$ 0.005)
Z = 30,000 ft
CG = 25%
$\Delta\ 0 = 0^{o}$ C

Fig. 28 shows a comparison between the measured C_X and the predicted C_X, based on the results of wind tunnel tests obtained with transition set off, from which we deduce $\Delta\ C_{X\ ext}$.

In general, we can observe good flight-wind tunnel accord: /20-11
Δ 100 $C_{X\ ext}$ between $\pm$ 2% of the drag (or thrust) of the plane.

There is a light dissipation in induced flight drag as compared to that of the wind tunnel.

The relatively substantial variation in these measurements (σ on Δ 100 $C_{X\ ext}$ σ 0.04 to 0.07) is explained by the precision of flight measurements (Δ 100 $C_{X\ ext}$ σ $\pm$ 0.03) and the engine variation relative to the average values as well as variations between planes (at M = 0.78 where practically only one plane is involved, variation is lower).

6.1.3 - Observations and Comments

We have not been able to find precise explanations for this flight/wind-tunnel difference. Such a difference is, nevertheless, within the precision limits of flight measurements and aerodynamic data.

We can make the following comments:

6.1.3.1 - Friction Drag

If, in order to go from wind tunnel tests to flight, we had employed Michel's formula wind-tunnel corrections would have been increased by Δ 100 C_X = -0.045, while with Winter's formula (see ref. 3) they would have been decreased by Δ 100 C_X = +0.015.

These different formulas are not equivalent. We must remember that the flight Reynolds number is about 20 times greater than the wind-tunnel Reynolds number.

6.1.3.2 - Influence of Altitude or of C_Z

Based on Mach number, there is a strong correlation between

$C_{Z\ meas}$ and flight altitudes.

The apparent induced drag dissipation can be explained in part by a reduction in thrust at a given regime which becomes greater as the altitude rises.

Therefore, at 35,000 ft., there will be a net thrust dissipation on the order of 2% (a 0.8% loss in raw thrust should be enough to explain it).

On the other hand, the analysis of the difference between measured oil flows and those calculated by means of the data sheet at N_1 flight regime shows flight consumption greater than predicted. Such consumption increases as the altitude rises; such variation is about 2% at 35,000 ft.

Under these conditions, it is necessary that, at fixed cruising speed and at 35,000 ft., the specific engine in-flight consumption is greater by 4% than that in the data sheet.

It would seem that this effect was discovered during tests on engines of this type carried out with altitude bench. To explain this C_Z evolution, we must recall the flexibility effect which could not be taken into account for lack of precise information regarding the repercussions such effect would have on the plane's drag.

However, the agreement between the measured equilibrium adjustments of the fixed plane and those predicted seems to confirm that the model shape is very similar to that of the plane in flight.

6.1.3.3 - Influence of Setting Off the Transition in Wind Tunnel

Fig. 29 compares directly flight results with predictions

originating from wind-tunnel results obtained with natural transition and set-off transition.

Despite the difficulties in calculating friction in natural transition, the precision is not bad: A 6% chord deviation on the transition line involves a difference of Δ 100 C_x S 0.01. This procedure will result in a reduction in predicted drag of 2% at M = 0.78 and of 3.5% at 0.82, thus increasing by as much the difference between prediction and flight.

I don't believe that we should abandon natural transition measurements.

The fact that the drag deviation between the two types of transition increases when the Mach rises is probably related to upper wing surface boundary layer shock interactions. Parietal displays show in effect that the shock is further back in natural transition that in set-off transition.

This unsolved problem becomes important in the study of /20-12 modern wing units where a good knowledge of the supersonic zone has considerable importance.

A possible solution consists in finding a way of obtaining in-flight Reynolds numbers on the model.

6.2 - Concorde

6.2.1 - Flight Measurements

The analysis presented here involves the preproduction 02 plane whose in-flight test equipment was best suited for the study of performances. The analysis was carried out in such a manner as to simplify the transposition to production planes the engines

of which are slightly different.

Therefore, according to the general outline in Fig. 27:
- parameter of gas generator operation: N_1 and C measured.

This means that the specific consumption mentioned in the engine data sheet will be found in flight at a given N_1. This should be true for the gas generator tested at the altitude bench.

- Individualized gas generator data sheet for each engine.
- Plane geometry: δ_9 measured for the plane
  δ_2 measured for the air intake.

Under these conditions, by using the in flight measurement precisions mentioned in Fig. 25, we can estimate the accuracy of independent parameters and infer the precision of $C_{X\ meas}$, C_X and, therefore, $\Delta C_{X\ ext}$.

Without taking into account the accuracy of propulsion data, but considering that of aerodynamic data, we arrive at an accuracy of Δ 100 $C_{X\ ext}$ on the order of $\pm$ 0.018.

Comment regarding nz

To analyze these tests, we have used the value measured by vertical accelerometer.

As shown in Fig. 30, the nz due to the g variation and the orbit effect can vary by 2%; with all things equal, a 1% decrease in nz corresponds to a decrease in drag of 0.7%.

Fig. 31 shows the accord between the calculated nz and those measured.

6.2.2 - Results

The shown results originate from 96 stabilized levels in the following flight regime:

$$1.91 < M < 2.04$$
$$48{,}000 \text{ ft} < z < 59{,}000 \text{ ft}$$
$$-15^{\circ} C < \Delta\theta < +10^{\circ} C$$
$$-3.8 < \delta q < +2.5$$
$$10.0 < 100\, C_{Z_A} < 14.1$$

Fig. 32 shows the results in the $\Delta C_{X\ ext}$ form as a function of two parameters, the correlation of which has been clearly evidenced at the beginning by means of static analysis, namely C_Z and $C_Z \cdot \delta q$.

a) Formula no. 1:
Initially the basic model had served to establish the aerodynamic data which represent the shape the plane should have in flight, half-cruising at $\delta q \simeq 0$; the construction frame was based upon it, taking into account the estimated rigidity of the structure.
The drag and elevator lift are those measured on the rigid model.
Based on these data, the first flight analysis was carried out.
The smoothing of $\Delta C_{X\ ext}$ gives formula no. 1.
One can observe the strong influence of C_{Z_A}, $\Delta\ 100\ C_{X\ ext} = 0.0035$ for $\Delta\ 100\ C_{Z_A} = 1$, indicating an in flight induced drag inferior to that found in wind tunnel and δq .

b) Formula no. 2:
Flights by the prototype plane have shown that the real structure rigidity is greater than that predicted at the start. /20-13
Special deformation measurements taken with the plane on the ground and in flight (cruising), have made it possible to re-

construct, for pre-production and production planes, the in flight shape at M = 2.0 for $\delta q \simeq 0$, based on the known structure shape.

A new basic model was designed to correspond to these new shapes and the aerodynamic data were modified by taking into account the differences measured with $\delta q = 0$ between the new and the original model.

Based on these new aerodynamic data, we have continued with the analysis of the same flight points; the smoothing of the corresponding $\Delta C_{X\ ext}$ gives formula no. 2.

We can observe that the influence of C_Z has greatly diminished, while that of δq has not changed; in order to understand this last point, we have undertaken a third analysis.

c) Formula no. 3

The aerodynamic data are the same as for the preceding case. Elevator drag as a function of α and δq is maintained, but the value of α, taken into account insteadof the value inferred from measurements on rigid model with in flight C_{Z_A}, is corrected by a $\Delta\alpha$ calculated by considering aeroelastic deformations for each measured value of δq different from 0.

Based on these new aerodynamic data, we have continued with the analysis of the same flight points; the smoothing of the corresponding $\Delta C_{X\ ext}$ gives formula no. 3.

We note that the influence of δq has been practically eliminated and that in the effective cruising zone the flight/wind tunnel variation means a completely independent $100\ \Delta C_{X\ ext}$, on the order of + 0.07 or 4% approximately of the plane's drag (or thrust).

This development only confirms the necessity of taking into account the flexibilty of such a plane.

The variation in measuring points is not affected by these different analysis procedures ($\lesssim$ on $\Delta\ 100\ C_{X\ ext} \simeq 0.01$)

and is in accord with the precision of flight measurements.

6.2.3 - Observations and Comments

As in the case of Airbus, we have not found a precise explanation for the flight/wind tunnel differences. Such difference seems greater than the flight measurement and aerodynamic data accuracy level.

We can make the following observations:

a) Influence of friction drag:
If, in going from wind tunnel tests to flight, we had used the Prandlt Schlichting or the Winter formulas (3), the corrections would have been lowered by Δ 100 C_X = 0.012, thus reducing by as much the flight/wind tunnel deficit. These different formulas are not equivalent. We must remember that the in flight Reynolds number is about three times greater than that in wind tunnel.

b) Influence of propulsion (air intake and secondary air):
An analysis of propulsion shows:
- for the air intake, an average performance deficit of $\Delta \eta_1 = 0.01$. This can help explain a Δ 100 $C_{X\ ext}$ of about 0.012.
- for the secondary air, the charge losses between the upstream side and the downstream side are, on the average, 30% greater than those predicted with the models. This can explain a Δ 100 $C_{X\ ext}$ of about 0.005.
- Secondary air bleeds: the measurements were carried out on the ground with pressure variations representing those in flight. However, the shape of the plane in flight and, consequently, of the nacelles and the relative positions of the various hatches could not be reconstructed.

If these bleeds were doubled (bleed hole per engine compartment, 10 cm instead of 5), the predicted C_X would be increased by $\Delta 100\ C_X \simeq 0.01$ and the $\Delta 100\ C_{X\ ext}$ reduced by as much. /20-14

c) Influence of gas generator and exhaust nozzle:
The motor mechanics carried out an analysis of in-flight results.
Without going into details, we can, nevertheless, state that a certain number of difficulties has emerged both at the gas generator level, this despite altitude bench tests, and at the exhaust nozzle level where wind-tunnel test conditions may be somewhat different from flight conditions.
We observe, in fact, problems similar to those found with Airbus.
Therefore, assuming that the air intake and the secondary air can explain 1% of the flight/prediction difference and that there is a doubt on the order of 1% as far as the friction drag and secondary air bleeds are concerned, a 2% net thrust deficit in the gas generator-exhaust nozzle combination (corresponding to 0.8% of raw thrust) will be enough to obtain good agreement between flight and prediction.

7 - Conclusion

The first conclusion we can make based on the Airbus and Concorde experiences is the knowledge of safety margins which should be taken when estimating cruising performances based on aerodynamic data resulting from wind-tunnel tests and propulsion data determined by present means, for a new subsonic or supersonic transport plane.

The other possibility is to plan the new plane by adding to the real performances of Airbus and Concorde the differences calculated on the basis of aerodynamic and propulsion data.

On the other hand, the study has demonstrated areas which are

in need of greater development. This has already been discussed in ref. 1.

a) Aerodynamic data:

At the present time, it is most important to improve testing in high subsonic and transsonic regimes, especially when aerodynamic gains in this field are the most valued.
A wind tunnel with a capacity for Reynolds numbers near to those in flight on a model having those dimensions utilized presently is indispensable to eliminate the influence of the boundary layer in the wind tunnel/flight transpositions, as well as in what involves the shape drag and the friction drag.
The second point is to be able to know the aeroelastic deformation effect (see thermoelastics in supersonic) on the measurements of a plane's polar curve.
The most direct way is to test different models (two or three at most) representing different shapes of the same plane.
On the other hand, in as much as it is difficult to conceive today of a substantial improvement in procedures for designing and weighing the models, except where motorized models are concerned where progress must be made in order to avoid having to integrate pressures, only a great number of tests on the same configuration will bring about a greater degree of reliability.
As a consequence, we can state that the average flight results for Airbus, based on 100 measurements, seem more reliable than the aerodynamic data inferred by the polar curve measured by Mach number.
Finally, we can doubt the validity of theoretical-empirical corrections relating to strays. However, I don't believe we can expect great progress in this area.

b) Propulsion data:

The flight/wind-tunnel difference occurring with Airbus and Concorde can be partially explained by a 1% deficit of the raw thrust. At this time there is no confirmation nor invalidation

of this hypothesis. I believe that it would be wise to present this difficult problem to specialists in order to find out the margin of uncertainty existing between oil flow, air flow and raw thrust in the gas generator-exhaust nozzle group.

c) Flight tests: /20-15

Test procedures for Airbus and Concorde were satisfactory for estimating global performance as long as a sufficiently high number of measuring points was taken during the flight.
On the other hand, improvements must be made to analyze in greater detail the causes of the flight/prediction differences. This concerns pressure and local temperature measurements the reliability of which has not always been very good.

REFERENCES

1. Pelagatti, C., Pilon, JC. and Bardaud J., Critical Analysis of Comparisons between Flight Results and Wind Tunnel Predictions for Subsonic and Supersonic Transport Planes, Agard CP, 187, 23.

2. Lievens, C., Estimation of Aerodynamic Coefficients Necessary for Calculation of Performances, Agard lecture series 56, section 4.

3. Leyman, C.S., Markham, T., Prediction of Supersonic Aircraft Aerodynamic Characteristics, Agard lecture series 67, section 5.

4. Hardy, J.M., Influence of Certain Characteristic Parameters on Ejectors Performances, Agard CP, 91, 11.

5. Saiz, M., Interaction of GE. CF6-50 Reactor Jets on the Airframe of Airbus in Cruising. Wind tunnel Simulation, AAAF 11th Applied Aerodynamics Conference.

6. Munniksma, B. and Jaarsma, F., Jet Interference of a Podded Engine Installation at Cruise Conditions, Agard CP, 150, 5.

7. Touraille, J. and Langlade, R., Measurement of Performances. In Flight Test Methods Applied to Concorde, Agard lecture series 38, section 7.

8. Love, William M., Current Wind Tunnel Accuracy Capability, 43rd semi-annual meeting of the Supersonic Tunnel Association, March, 1975.

EQUATIONS D'EQUILIBRE EN CROISIERE

1

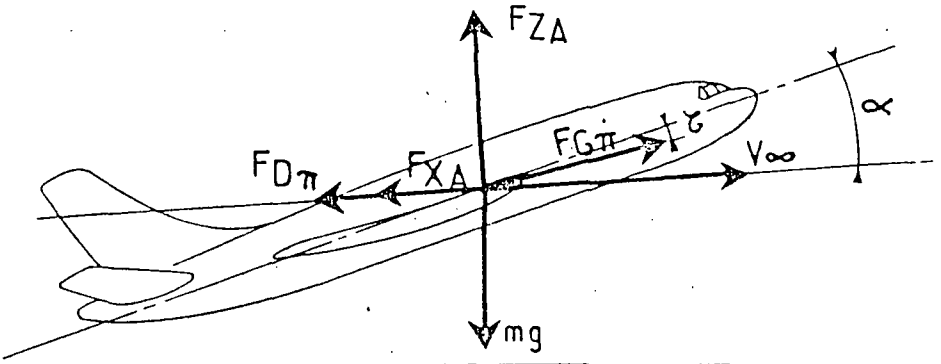

$n_x.mg$	$= F_{X_A}$	$+ F_{D\pi} - F_{G\pi}.\cos(\alpha + \gamma)$
$n_z.mg$	$= F_{Z_A}$	$+ F_{G\pi}.\sin(\alpha + \gamma)$
$\frac{d(mg)}{dt}$	$=$	C
2 Données ou mesures avion	3 Données aérody-namiques	4 Données propulsion

5 en croisière n_x, α, γ petits, $nz \# 1$

$$\begin{cases} F_{X_A} \# -F_{D\pi} + F_{G\pi} \\ F_{Z_A} \# mg \\ C \# cs(F_{G\pi} - F_{D\pi}) = cs\, F_{X_A} \end{cases}$$

6 rayon d'action spécifique

$$SR = \frac{\Delta X}{\Delta(mg)} = \frac{V}{C} = \frac{1}{mg}.\frac{V.mg}{C} \# \frac{1}{mg}.\frac{V}{cs}\varphi$$

Fig. 1

Key: 1. Equilibrium equations at cruise conditions
2. Data or measurements for plane
3. Aerodynamic data
4. Propulsion data
5. At cruise conditions
6. Specific range of action

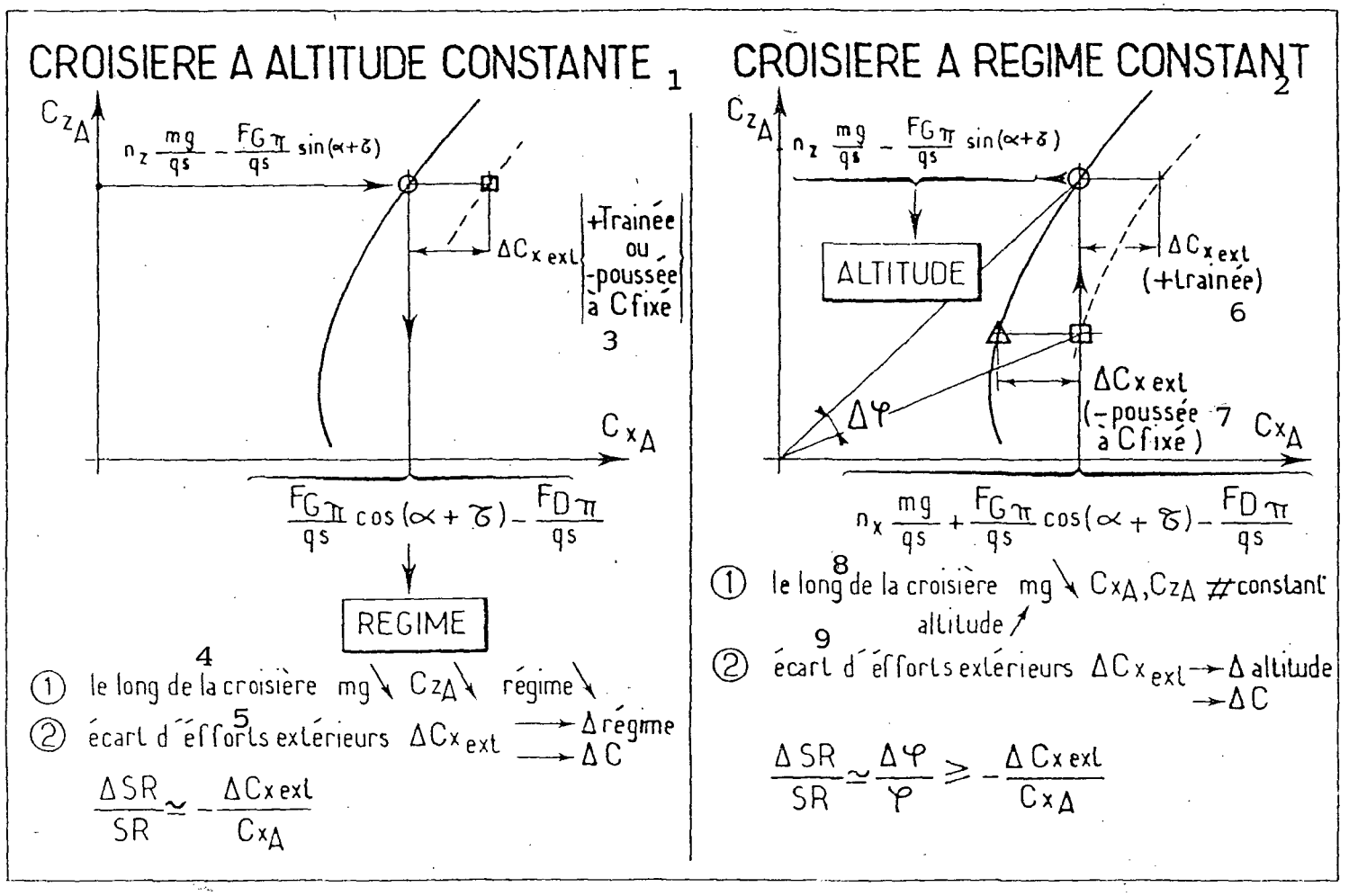

Fig. 2.

Key:
1. Cruising at constant altitude
2. Cruising at constant regime
3. Drag or thrust at fixed C
4. Length of cruising regime
5. Variation of external stresses
6. Drag
7. Thrust at fixed C
8. Length of cruising regime
9. Variation of external stresses

EFFECT OF 1% DRAG INCREASE (OR THRUST DECREASE) AT CRUISE CONDITIONS

IMPOSED LIMITS		SUBSONIC PLANE		CONCORDE
		Dest. 2500 nm = 270 passang	Dest. 5100 nm = 300 Passang.	Dest 3200 nm ISA + 5 = 100 Passang
TAKE-OFF MASS	Necessary fuel Commercial load	+0,6 % -0,9 % ⇒ $\frac{\Delta DOC}{DOC}$ = +1,2 %	+0,7 % -2,4 % ⇒ $\frac{\Delta DOC}{DOC}$ = +2,7 %	+0,6 % -4,8 % ⇒ $\frac{\Delta DOC}{DOC}$ = + 5 %
COMMERCIAL LOAD	Necessary fuel	+0,8 % ⇒ $\frac{\Delta DOC}{DOC}$ = +0,3 %	+0,9 % ⇒ $\frac{\Delta DOC}{DOC}$ = +0,3 %	+1,2 % ⇒ $\frac{\Delta DOC}{DOC}$ = +0,3 %
TANK CAPACITY	Commercial load	-5,6 % ⇒ $\frac{\Delta DOC}{DOC}$ = +6,1 %	-7,8 % ⇒ $\frac{\Delta DOC}{DOC}$ = +8,6 %	-13,1 % ⇒ $\frac{\Delta DOC}{DOC}$ = +14,2 %

Fig. 3.

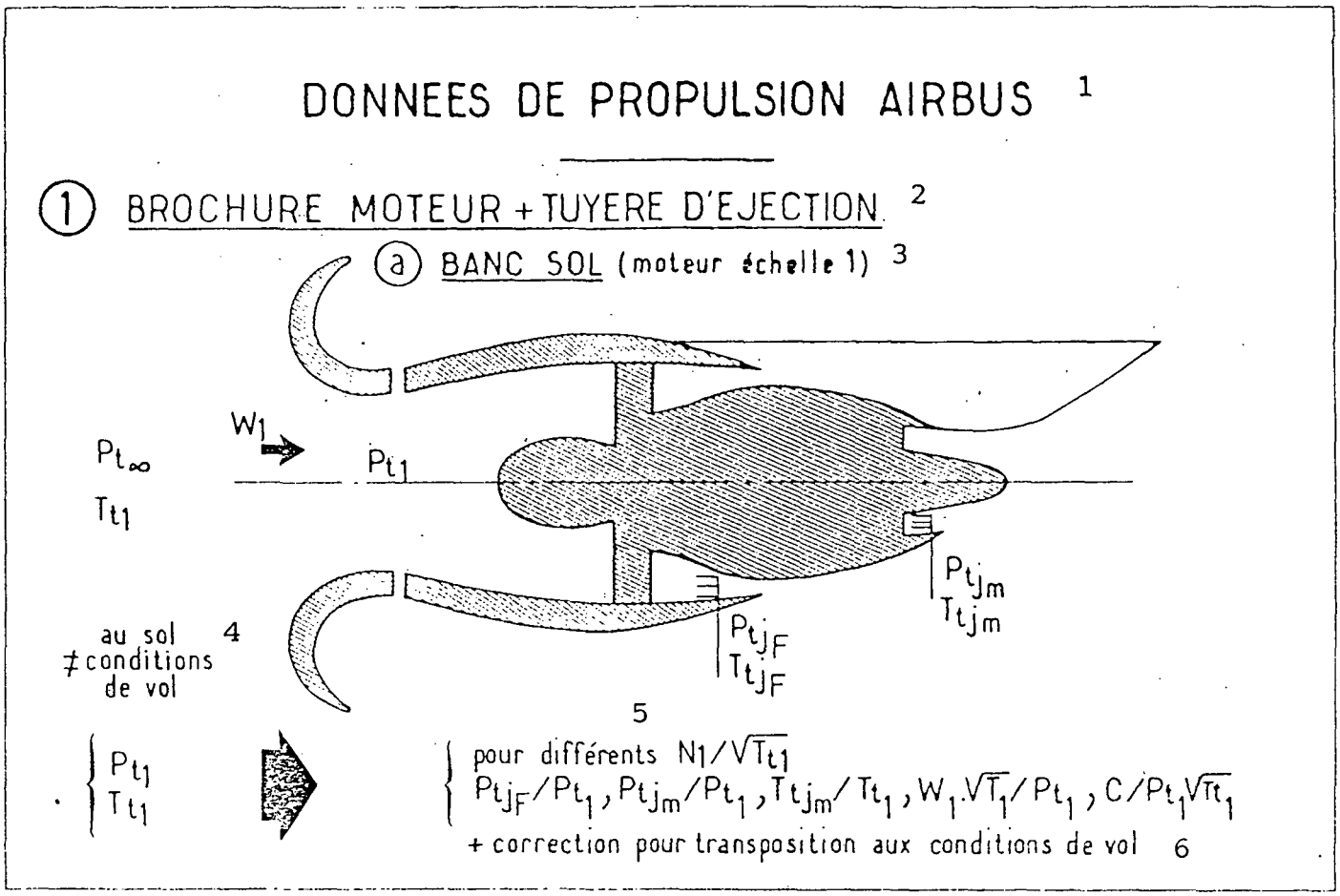

Fig. 4.

Key:
1. Airbus propulsion data
2. Data sheet for engine/exhaust nozzle
3. Ground bench (scale 1 engine)
4. On ground ≠ from flight conditions
5. For different...
6. + correction for transposition to flight conditions

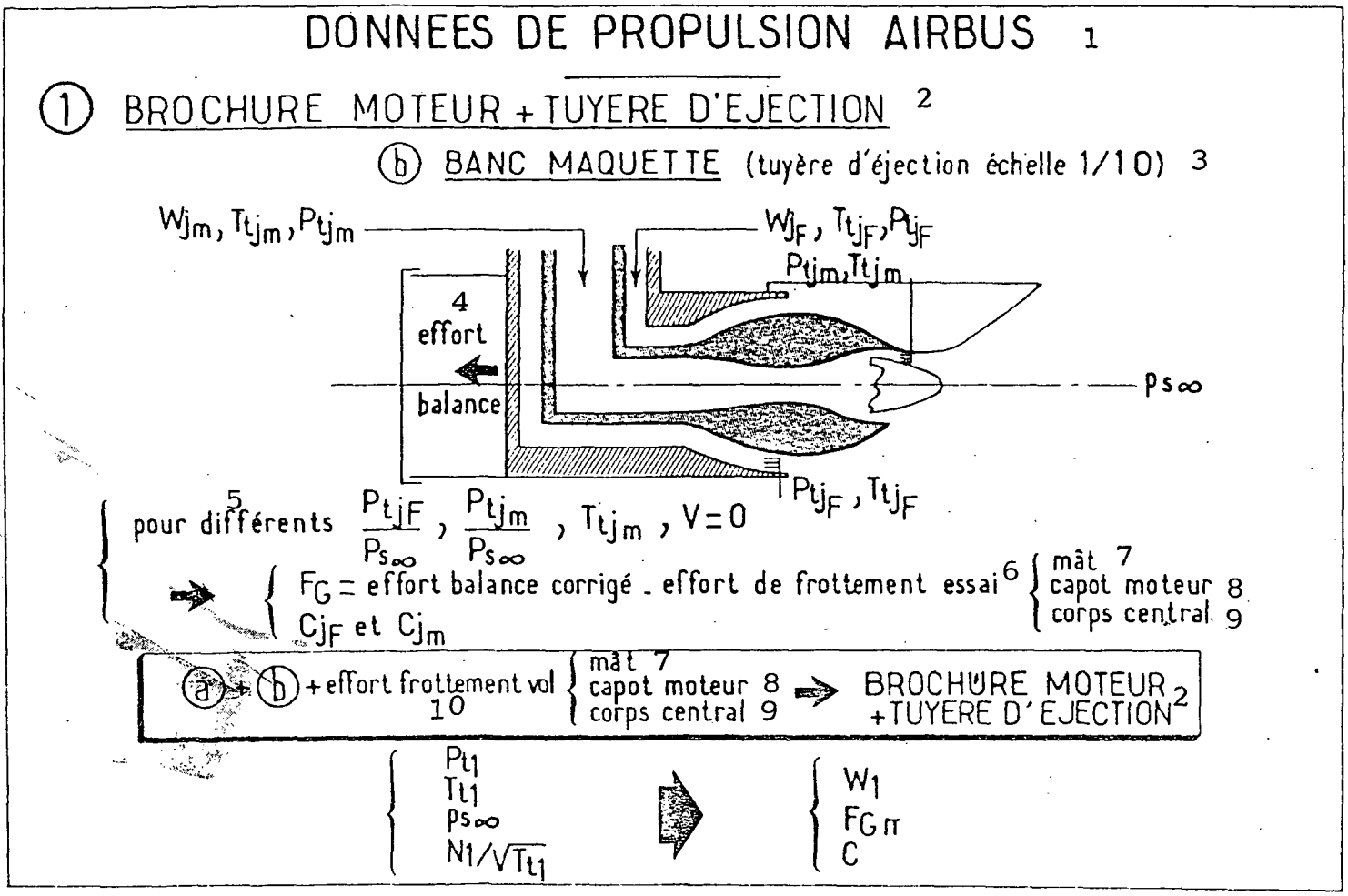

Fig. 4b.

Key:
1. Airbus propulsion data
2. Data sheet for engine/exhaust nozzle
3. Model bench (scale 1/10 exhaust nozzle)
4. Stress
5. For different...
6. Corrected balance stress - friction stress during test
7. Strut
8. Cowl
9. Central body
10. Friction stress in flight

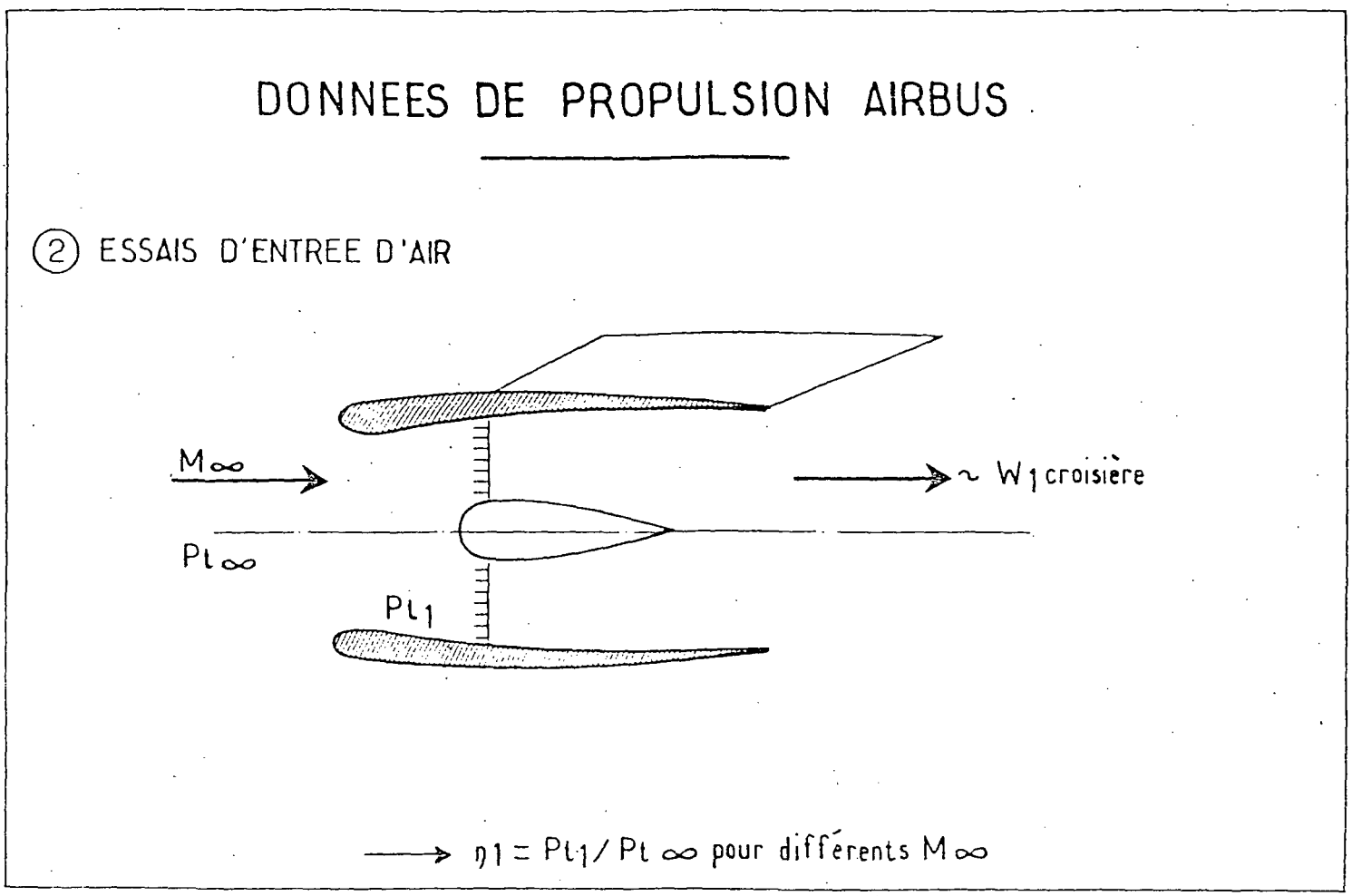

Fig. 5.

Key: 1. Airbus propulsion data
2. Air intake tests
3. Cruising
4. For different...

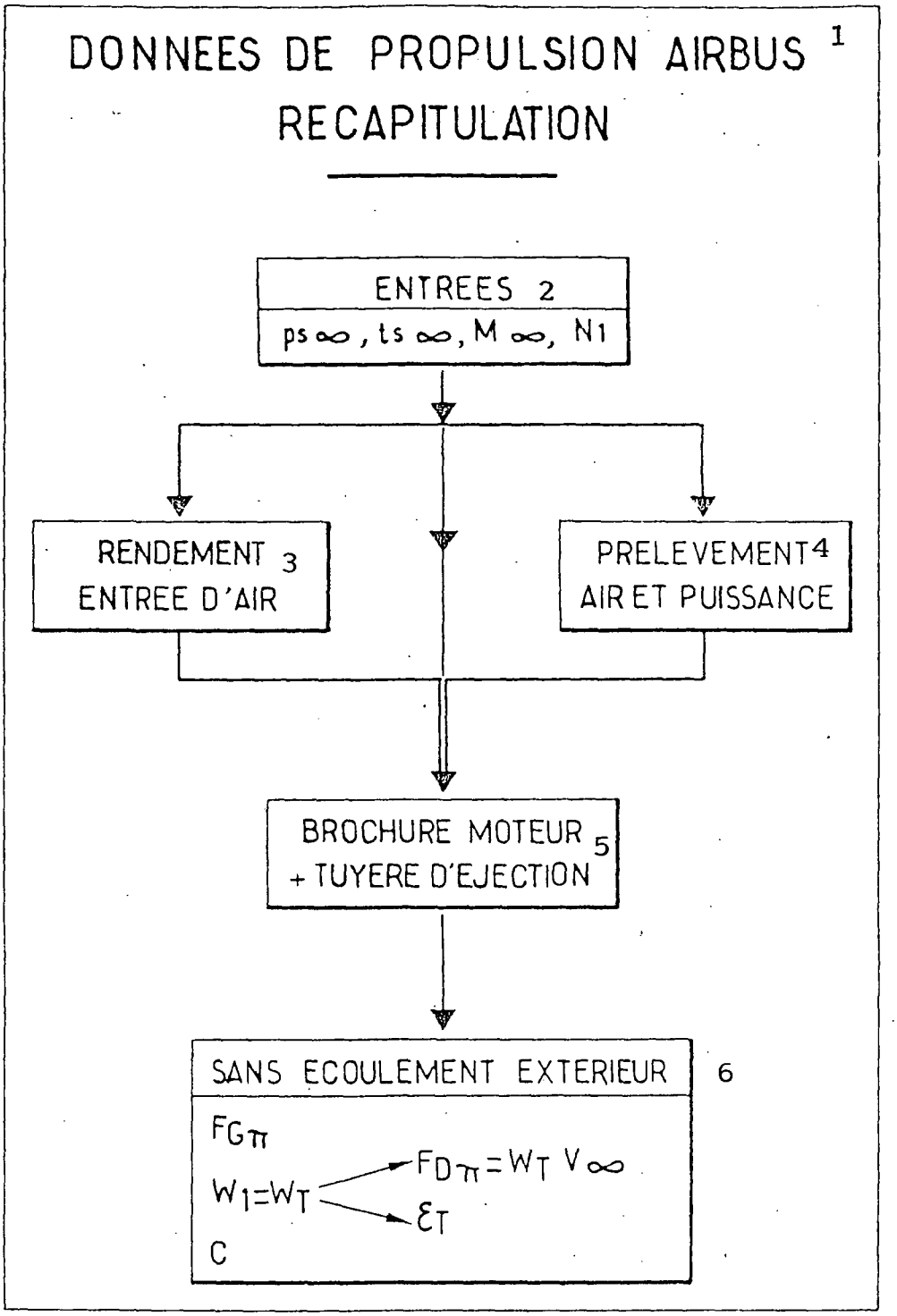

Fig. 6.

Key: 1. Airbus propulsion data
2. Inlets
3. Air intake efficiency
4. Collection air and power
5. Data sheet for engine/exhaust nozzle
6. Without external flow

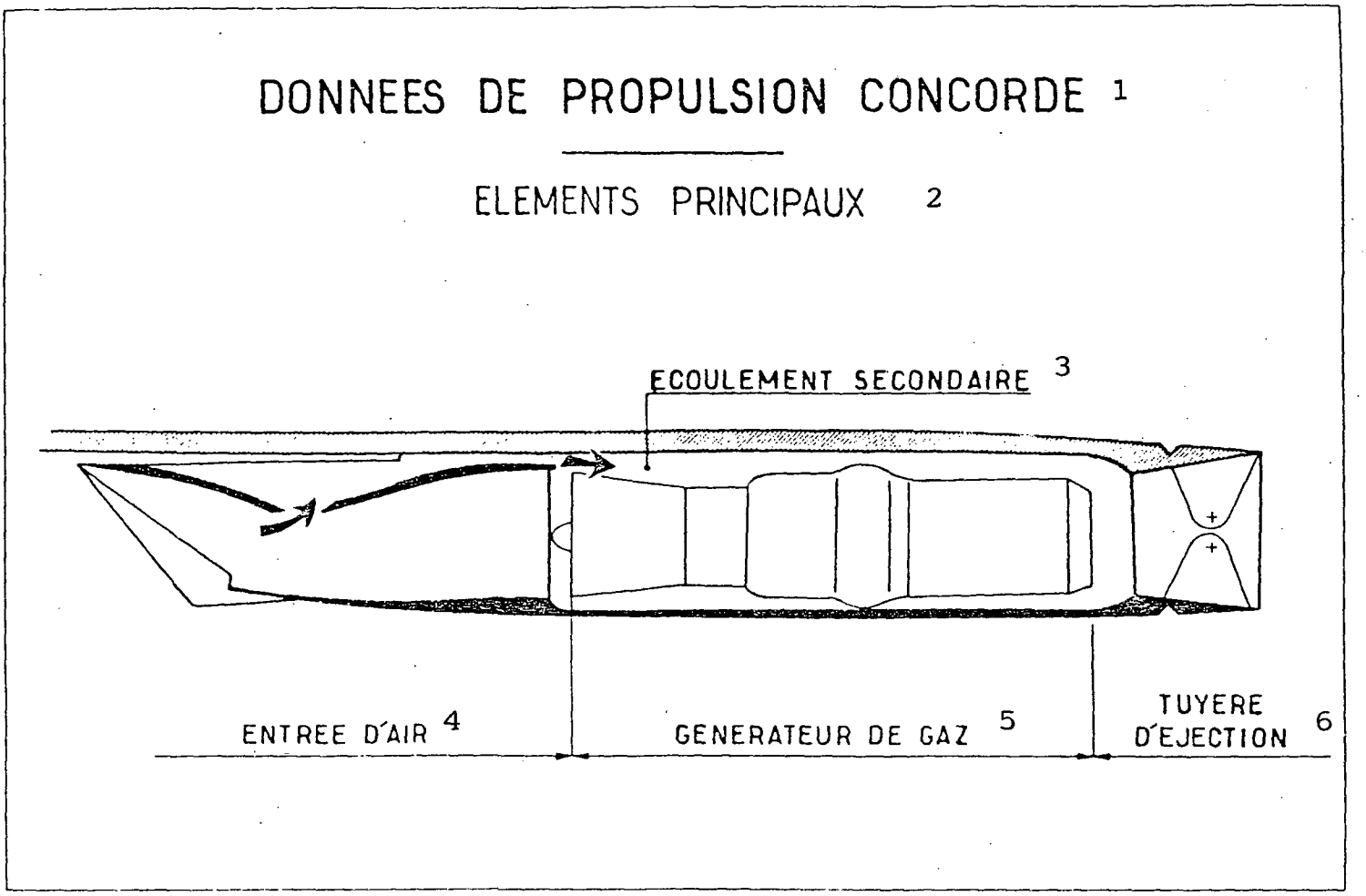

Fig. 7.

Key: 1. Concorde propulsion data
2. Main components
3. Secondary flow
4. Air intake
5. Gas generator
6. Exhaust nozzle

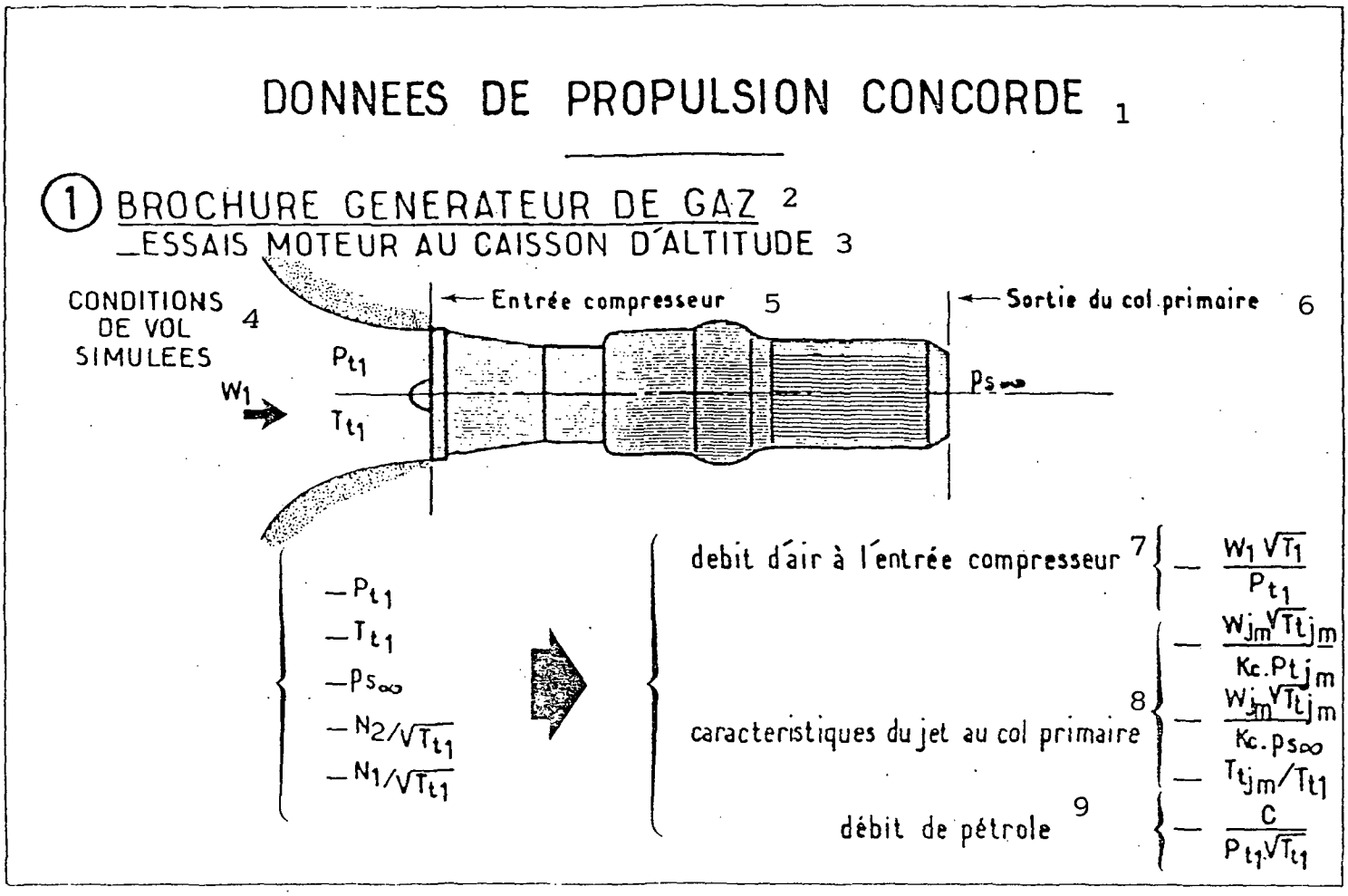

Fig. 8.

Key:
1. Concorde propulsion data
2. Data sheet for gas generator
3. Engine tets on altitude bench
4. Simulated flight conditions
5. Compressor inlet
6. Primary nozzle outlet
7. Air flow at compressor inlet
8. Jet characteristics at primary nozzle
9. Oil flow

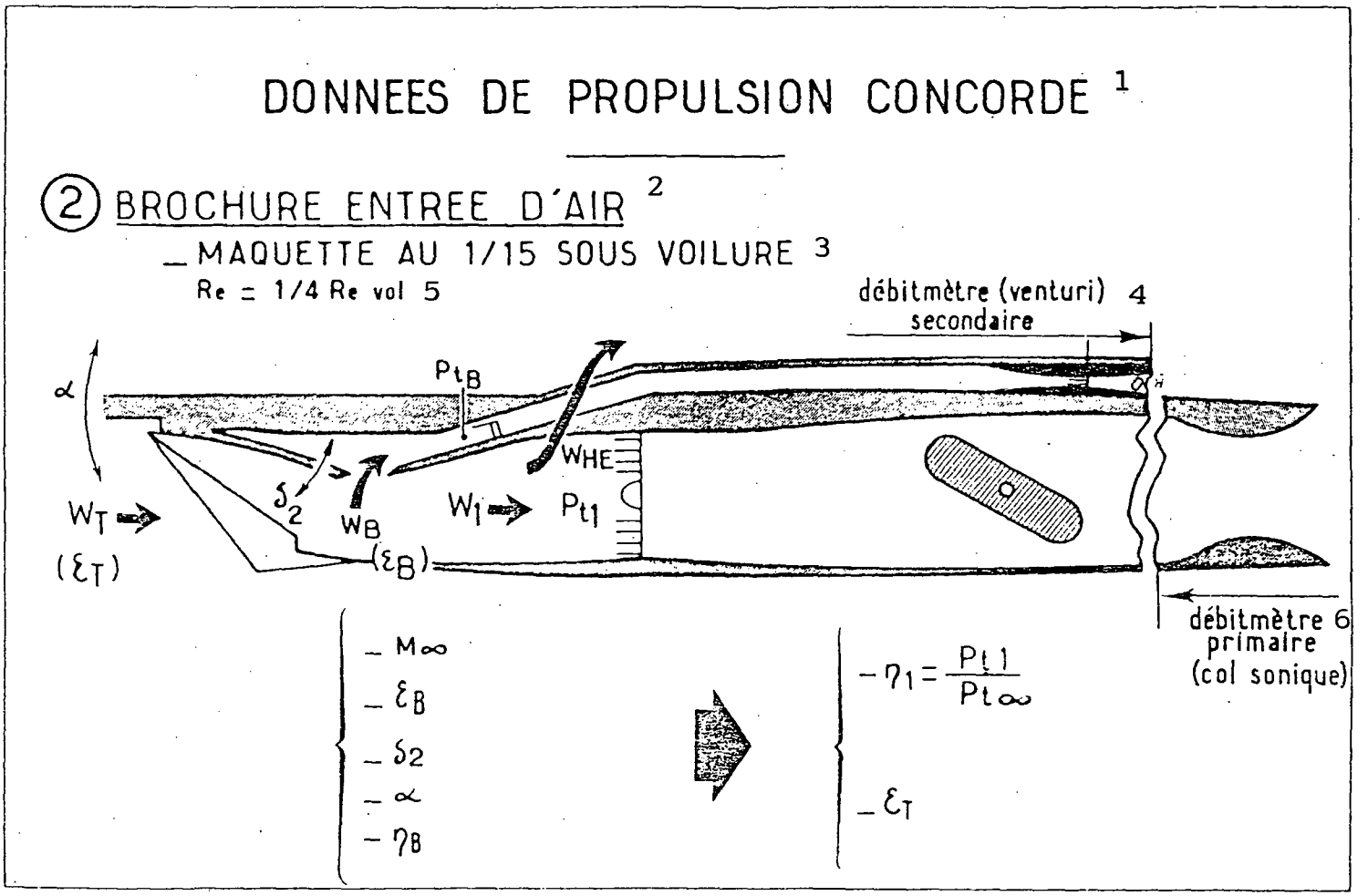

Fig. 9.

Key:
1. Concorde propulsion data
2. Air intake data sheet
3. 1/15 scale under wing unit model
4. Secondary flowmeter (venturi)
5. Flight
6. Primary flowmeter (sonic nozzle)

DONNEES DE PROPULSION CONCORDE [1]

(3) BROCHURE TUYERE [2]

(a) Référence = forme et jet homologue à la maquette planeur. [3]

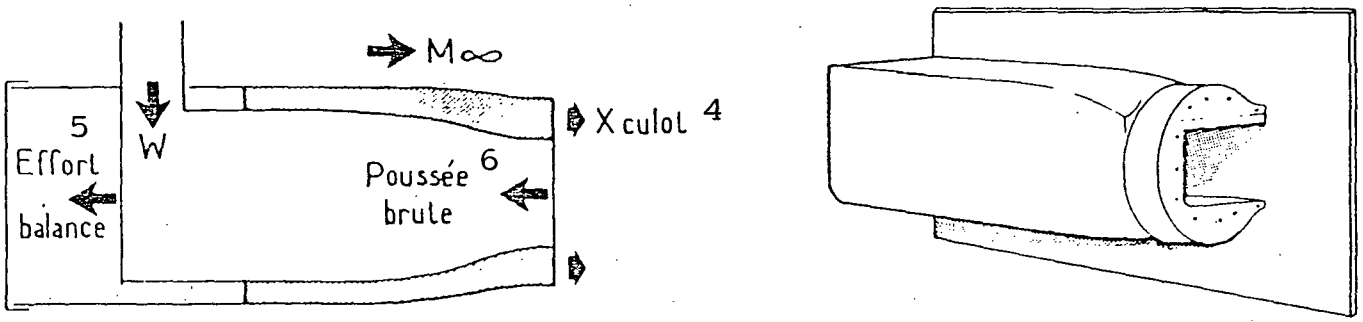

F_{ref} = Effort balance corrigé + poussée brute - effort culot. [7]

Fig. 10a.

Key:
1. Concorde propulsion data
2. Nozzle data sheet
3. Reference = shape and jet identical to model of plane
4. Base
5. Balance stress
6. Raw thrust
7. F_{ref} = corrected balance stress + raw thrust - base stress

DONNEES DE PROPULSION CONCORDE [1]

③ BROCHURE TUYERE [2]

ⓑ Forme et jet réel [3]

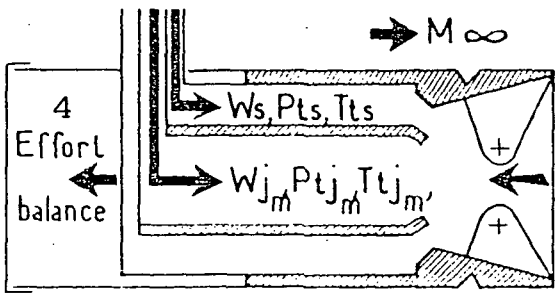

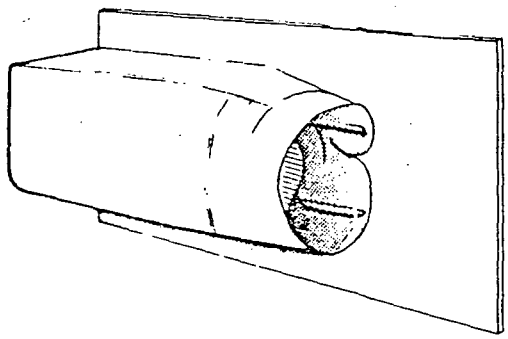

Ft = Effort balance corrigé – F frottement du jet sur plaque + correction gaz chaud – recalage interne [6]

ⓐ + ⓑ ➡ brochure tuyère [2]

$-W_{j_m}\sqrt{T_{tj_m}} / K_c p_{tj_m}$

$-W_{j_m}\sqrt{T_{tj_m}} / K_c p_{s\infty}$

$-M_\infty$

$-\mu = W_S \sqrt{T_{tS}} / W_{j_m}\sqrt{T_{tj_m}}$

➡ $F_{G\pi} = F_T - F_{ref}$

P_{ts} / P_{tj_m}

Fig. 10b.

Key:
1. Concorde propulsion data
2. Nozzle data sheet
3. Actual shape and jet
4. Balance stress
5. Raw thrust
6. Ft = Corrected balance stress - F jet friction on plate + hot gas correction - internal adjustment

DONNEES DE PROPULSION CONCORDE [1]

(4) BROCHURE ECOULEMENT SECONDAIRE [2]
(maquette échelle 1/2) [3]

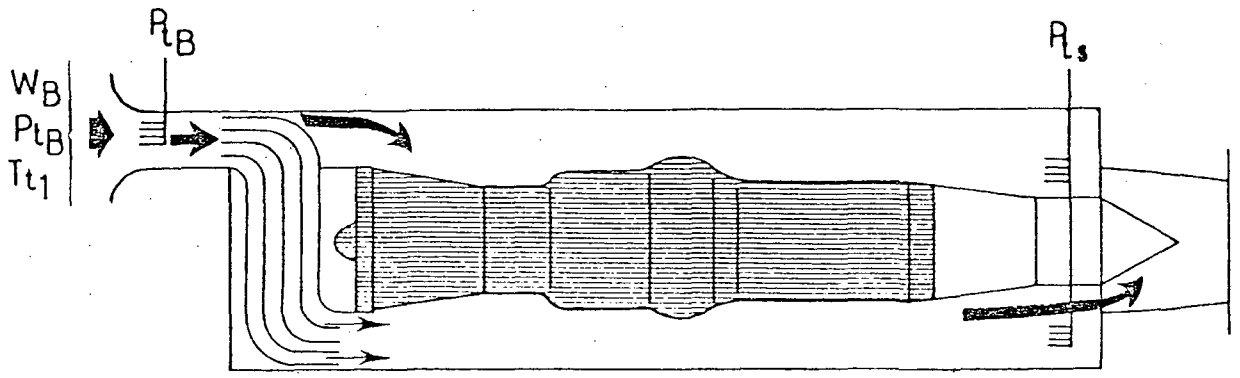

$$\frac{W_B\sqrt{T_{t_1}}}{P_{t_B}} \Rightarrow \frac{P_{t_s}}{P_{t_B}}$$

Fig 11.

Key: 1. Concorde propulsion data
2. Data sheet for secondary flow
3. 1/2 scale model

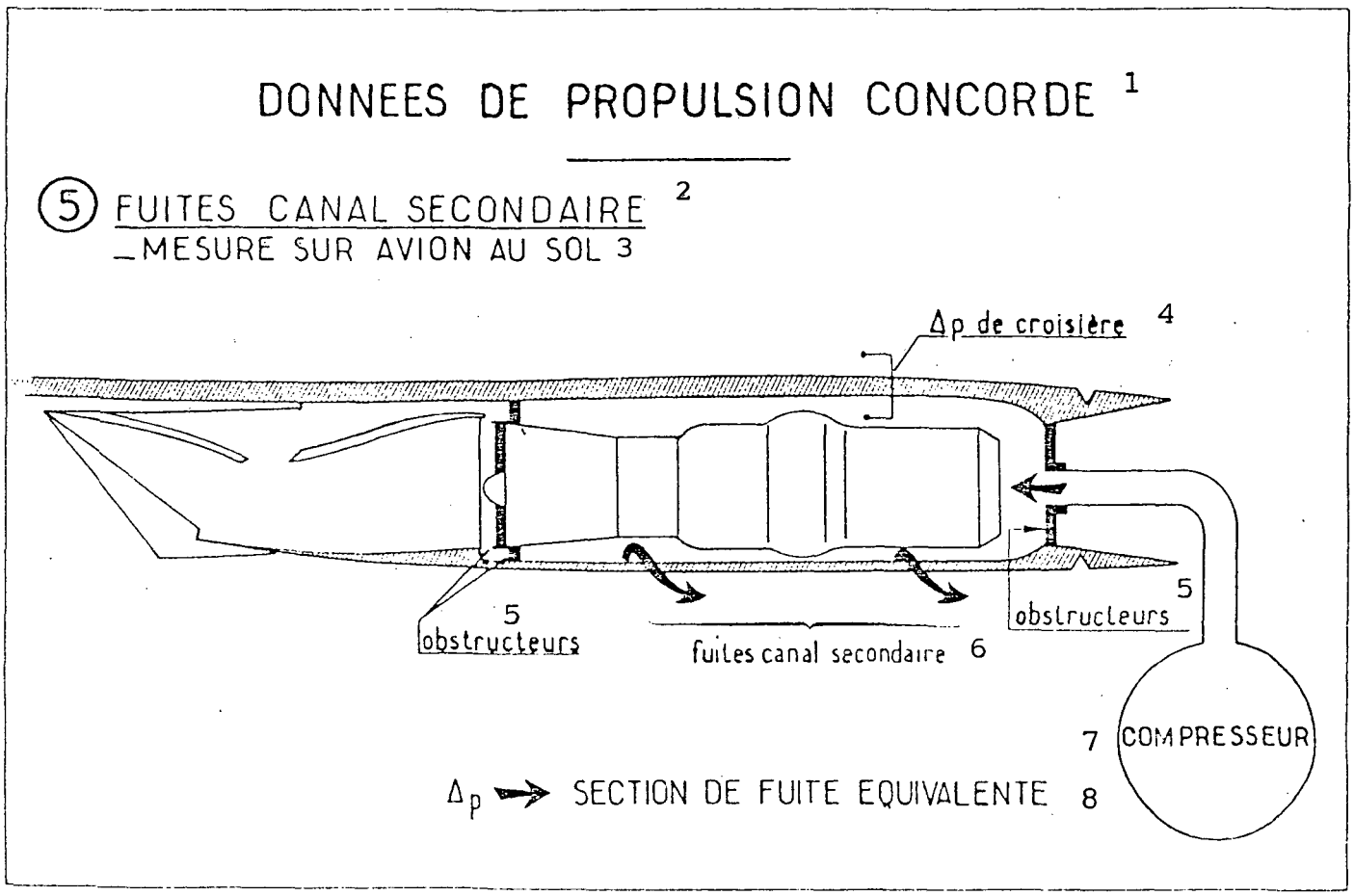

Fig. 12.

Key: 1. Concorde propulsion data
2. Secondary duct bleeds
3. Ground measurements on plane
4. Δ p in cruising
5. Chokes
6. Secondary duct bleeds
7. Compressor
8. Equivalent bleed section

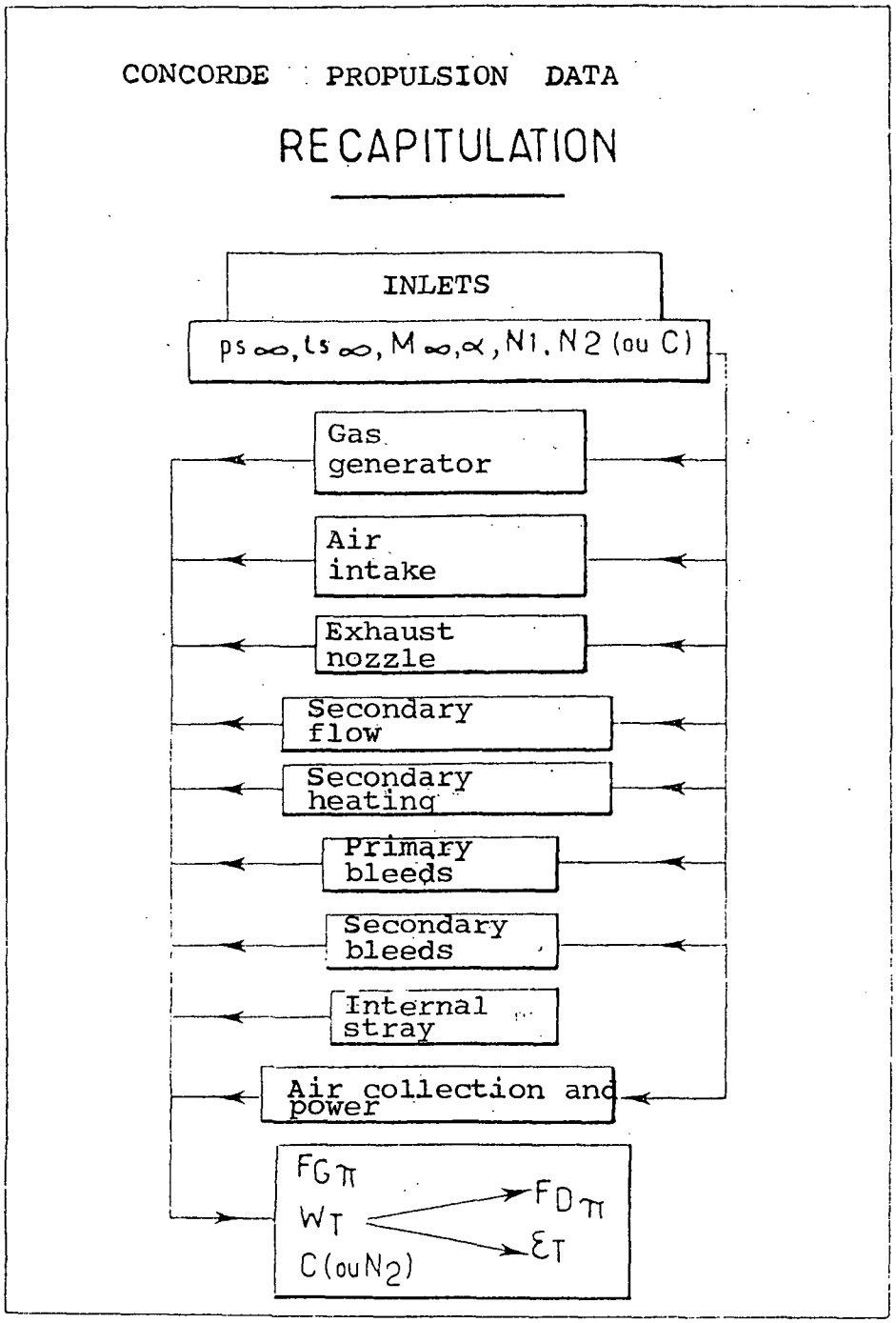
CONCORDE PROPULSION DATA
RECAPITULATION
INLETS
ps∞, ts∞, M∞, α, N1, N2 (ou C)
Gas generator
Air intake
Exhaust nozzle
Secondary flow
Secondary heating
Primary bleeds
Secondary bleeds
Internal stray
Air collection and power
FGπ
WT
C(ouN2)
FDπ
εT

Fig. 13.

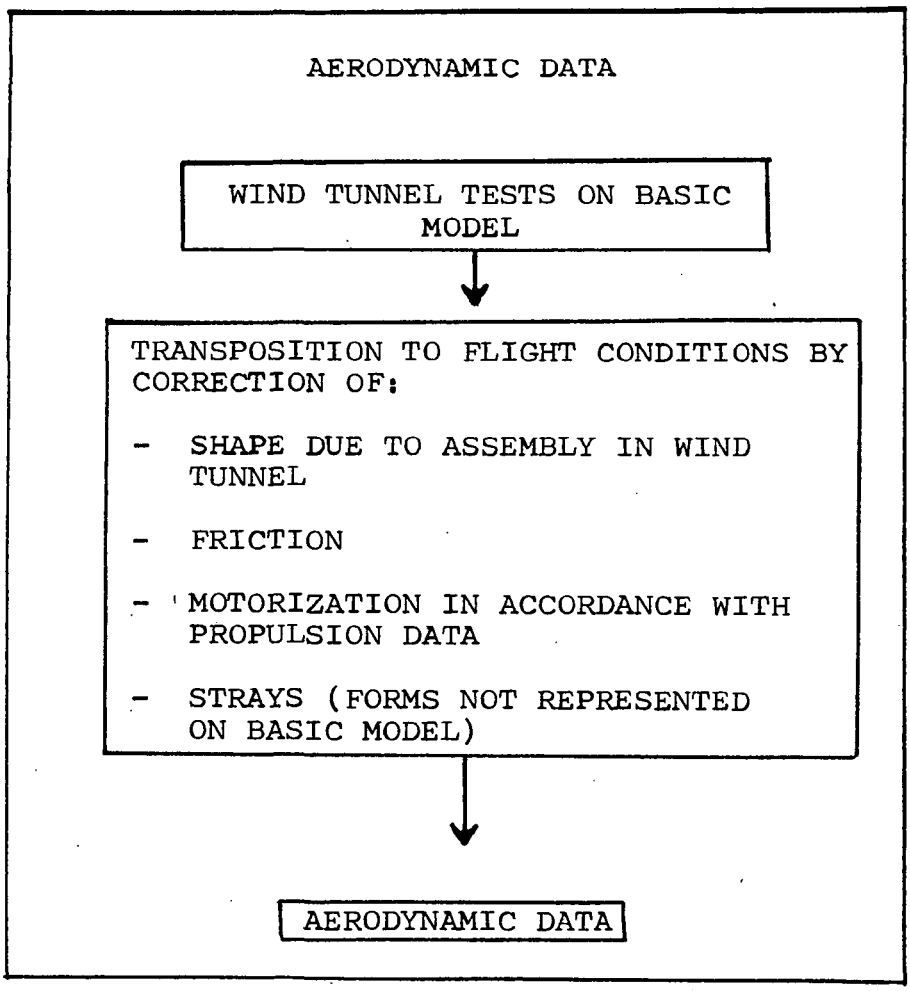
AERODYNAMIC DATA
WIND TUNNEL TESTS ON BASIC MODEL
TRANSPOSITION TO FLIGHT CONDITIONS BY CORRECTION OF:
- SHAPE DUE TO ASSEMBLY IN WIND TUNNEL
- FRICTION
- MOTORIZATION IN ACCORDANCE WITH PROPULSION DATA
- STRAYS (FORMS NOT REPRESENTED ON BASIC MODEL)
AERODYNAMIC DATA

Fig. 14.

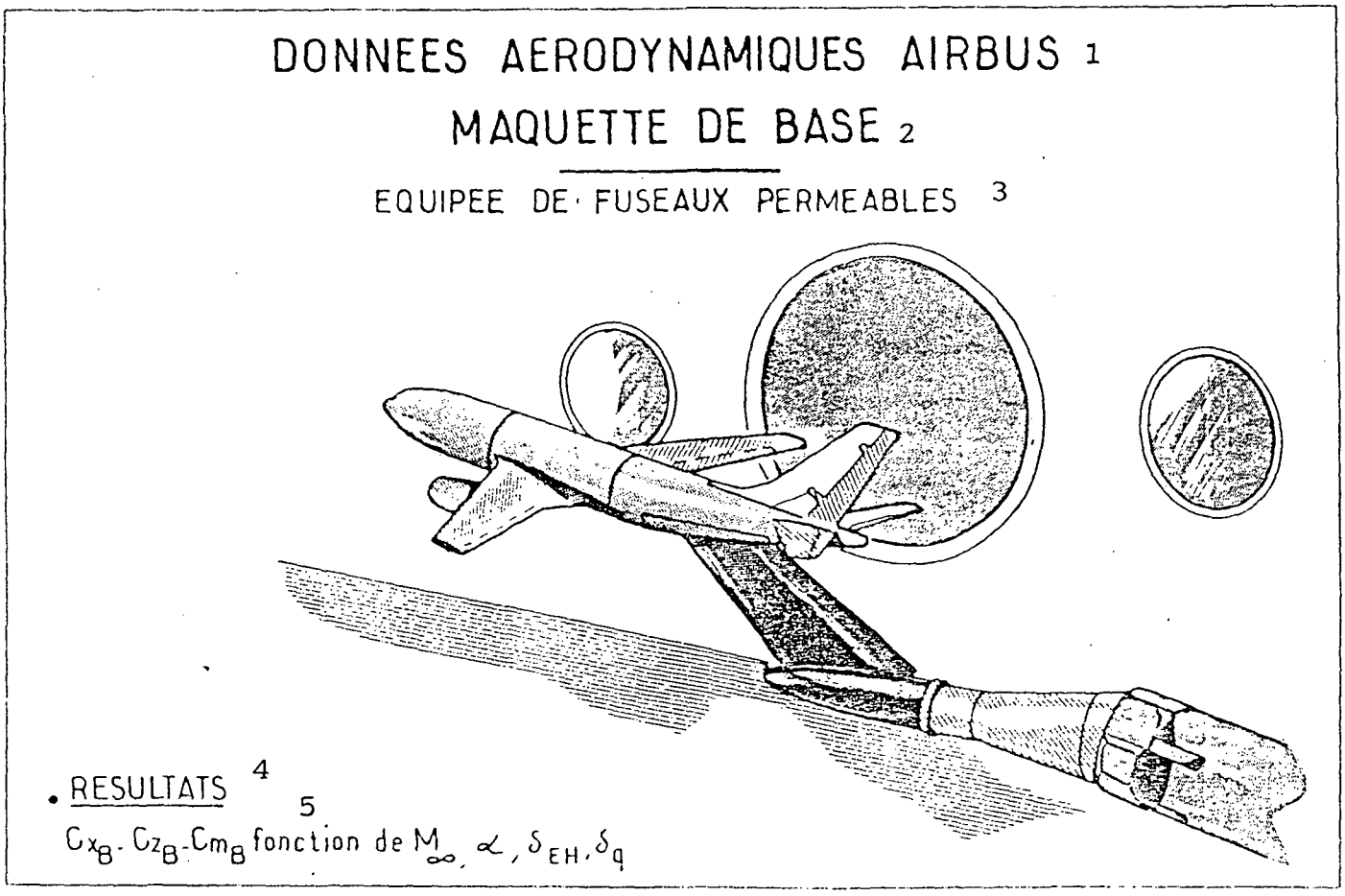

Fig. 15.

Key: 1. Airbus aerodynamic data
2. Basic model
3. Equipped with permeable pods
4. Results
5. ... as a function of...

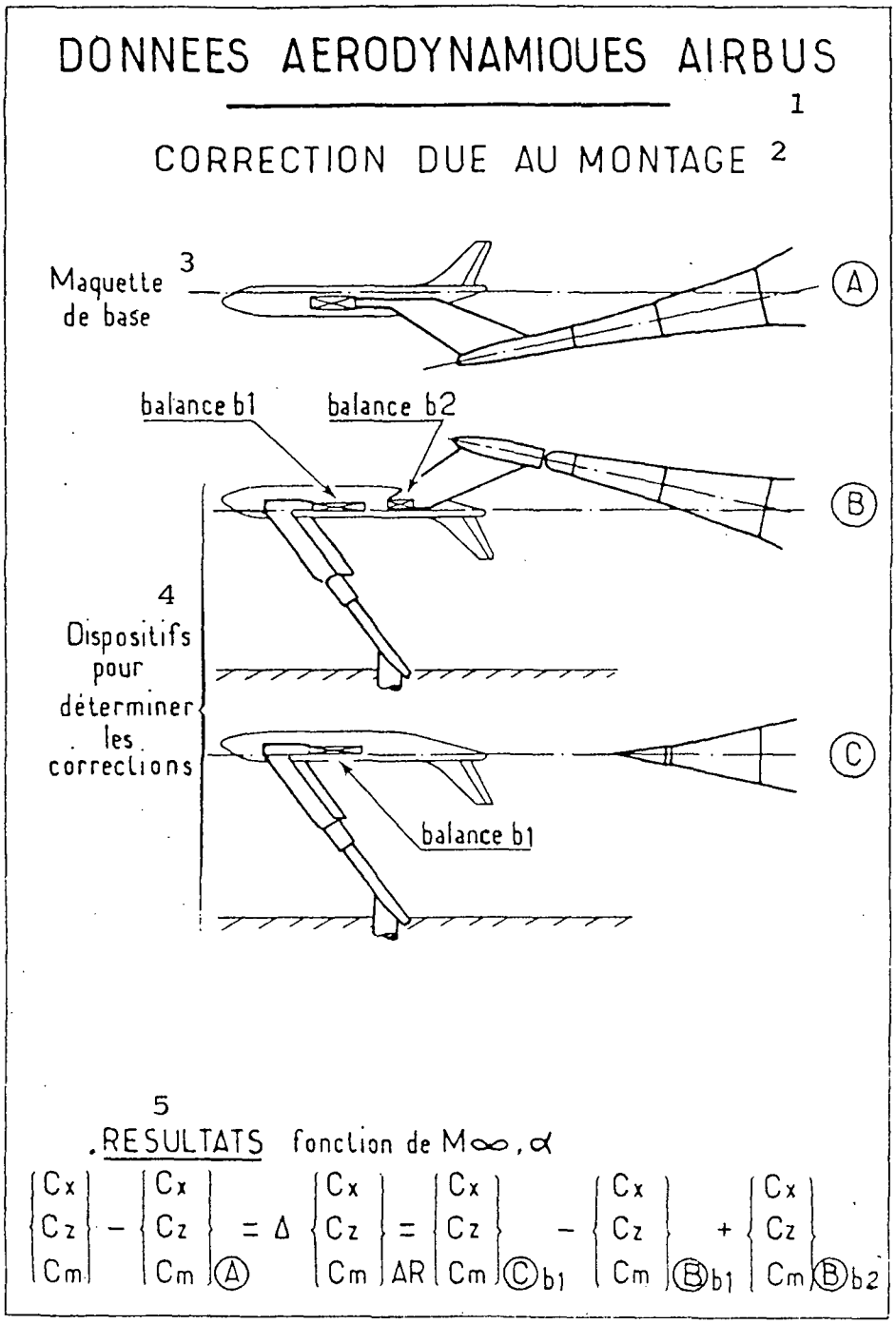

Fig. 16.

Key: 1. Airbus aerodynamic data
2. Correction due to assembly
3. Basic model
4. Devices for determining corrections
5. Results as a function of...

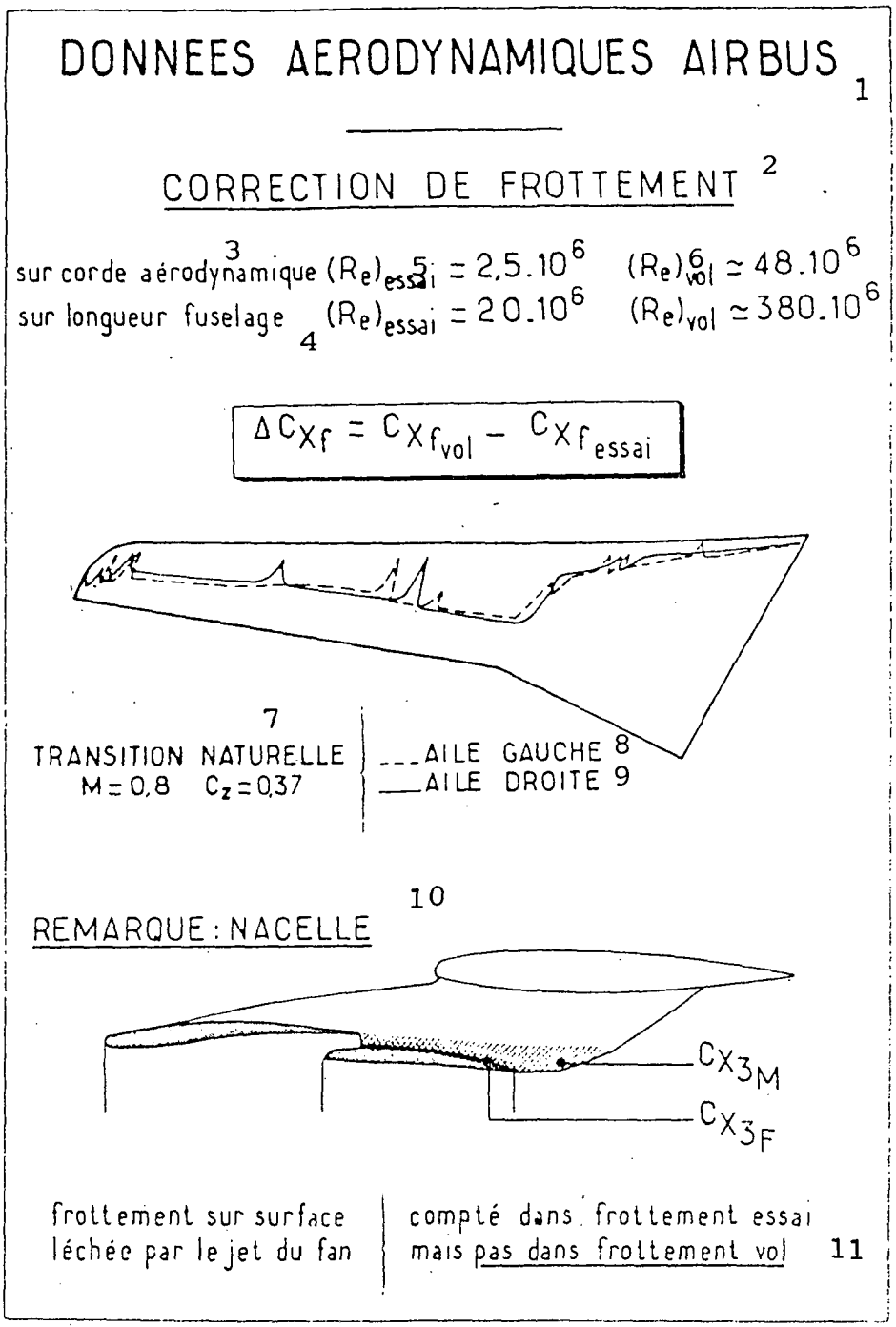

Fig. 17.

Key:
1. Airbus aerodynamic data
2. Friction correction
3. On aerodynamic chord
4. On fuselage length
5. Test
6. Flight
7. Natural transition
8. Left wing
9. Right wing
10. Note: nacelle
11. Friction on surface touched by fan jet { considered in friction test, but not in flight

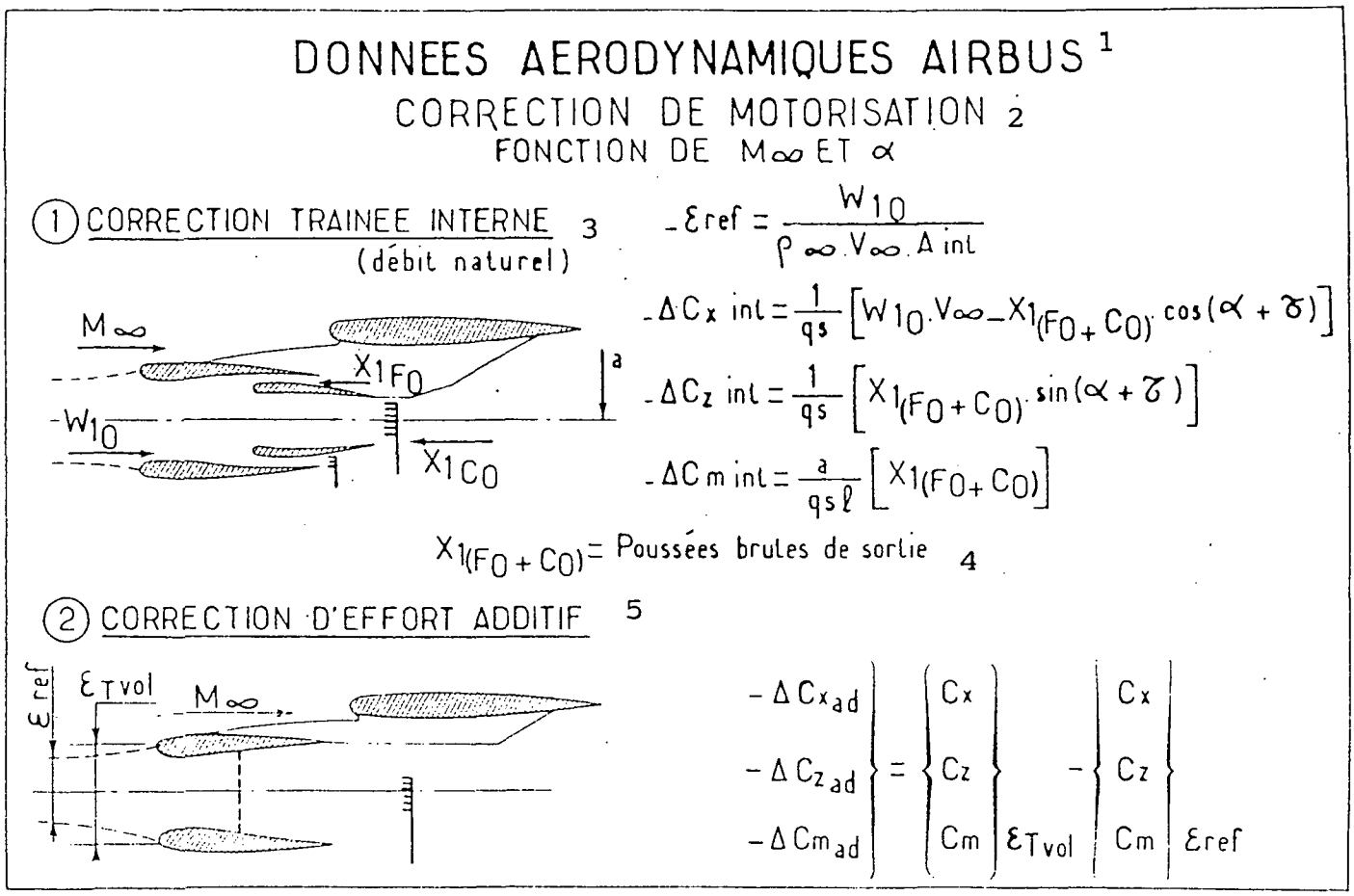

Fig. 18a.

Key: 1. Airbus aerodynamic data
2. Motorization correction as a function of M ∞ and α
3. Internal drag correction (natural flow)
4. Raw outlet thrusts
5. Additive stress correction

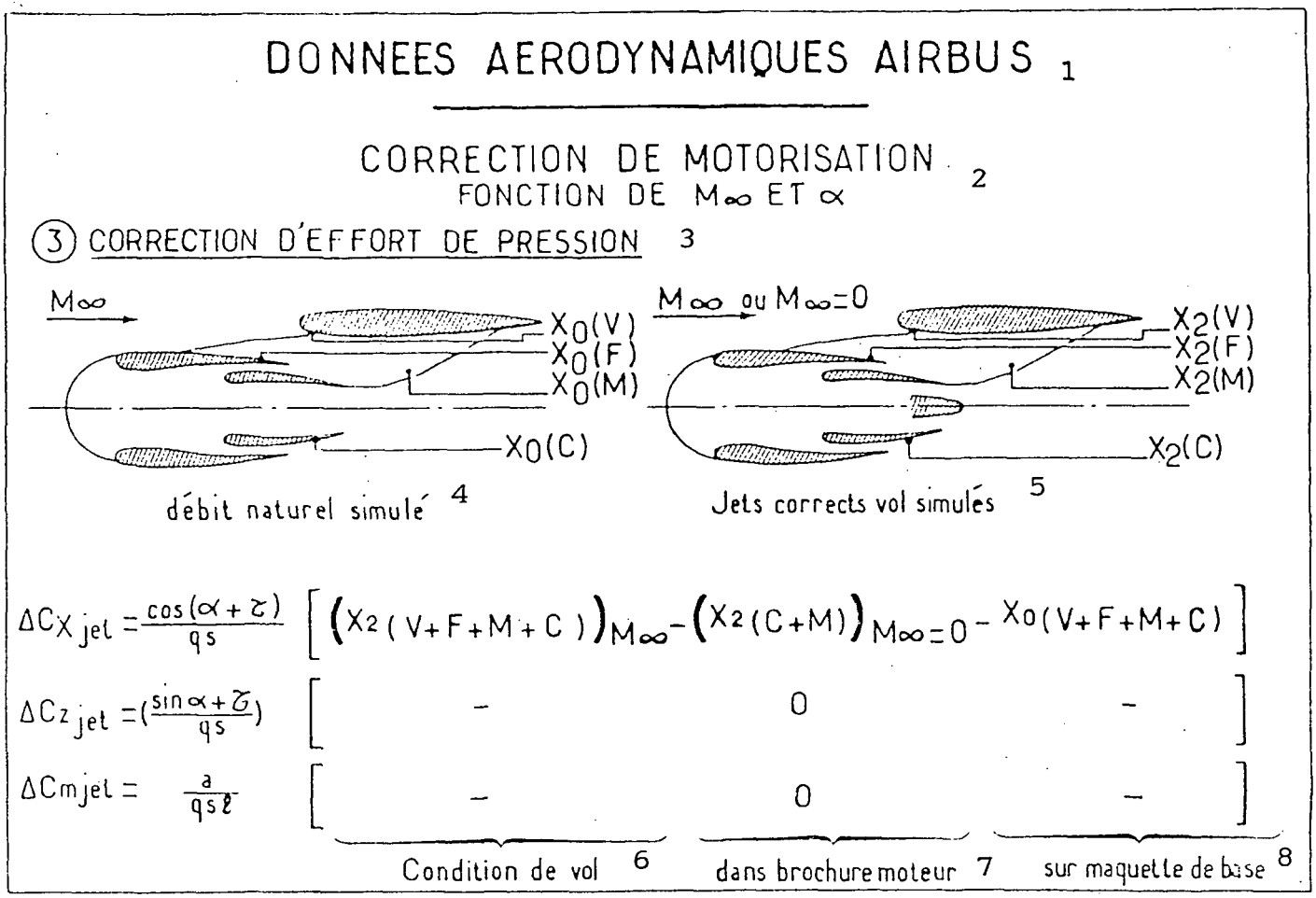

Fig. 18b.

Key:
1. Airbus aerodynamic data
2. Motorization correction as a function of M_∞ and α
3. Pressure stress correction
4. Simulated natural flow
5. Simulated corrected flight jets
6. Flight condition
7. In engine data sheet
8. On basic model

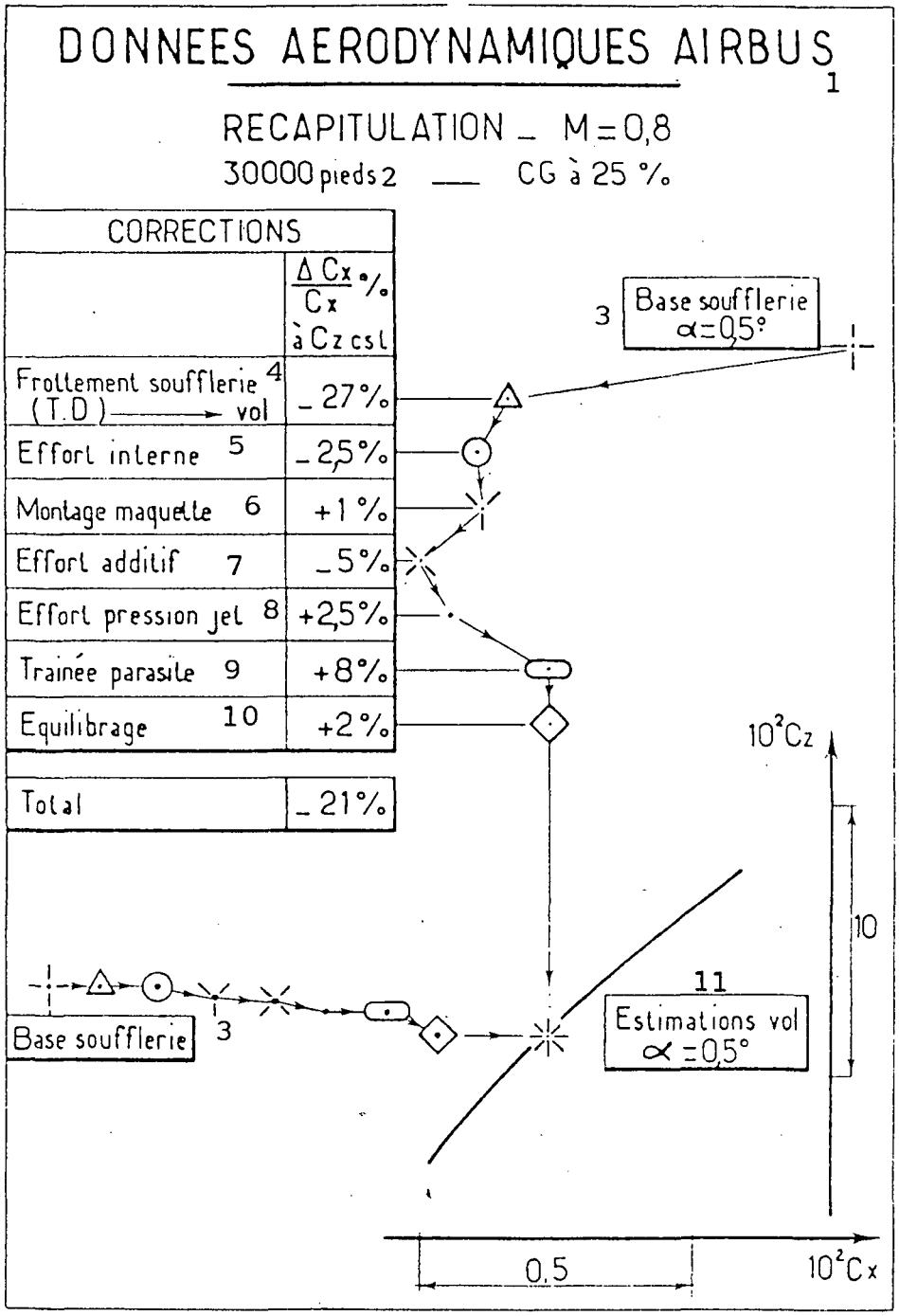

Fig. 19.

Key: 1. Airbus aerodynamic data
2. 30,000 ft.
3. Wind tunnel course
4. Wind tunnel friction - (T.D.) flight
5. Internal stress
6. Model assembly
7. Additive stress
8. Jet pressure stress
9. Stray drag
10. Trim 11. Flight estimations

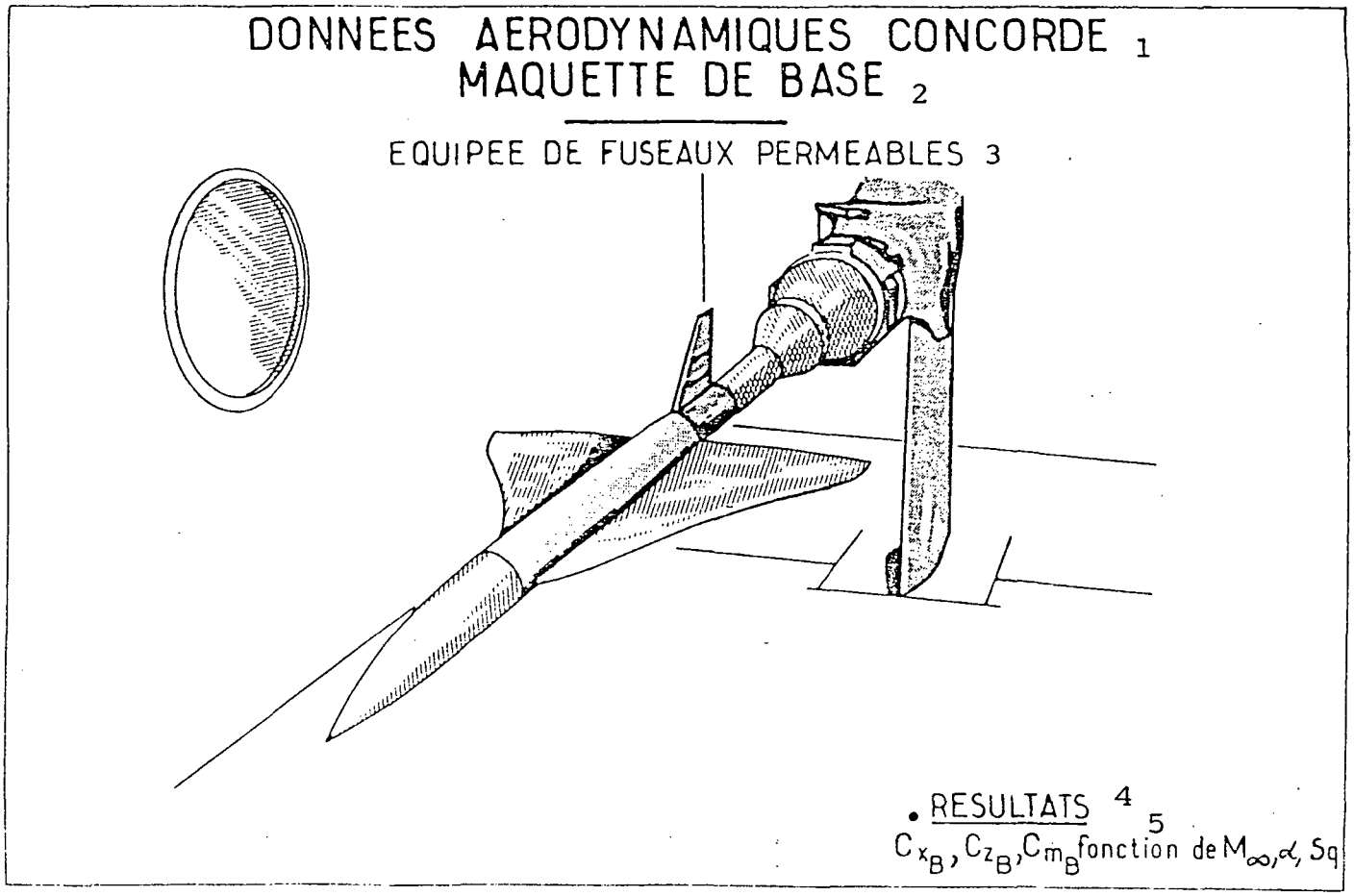

Fig. 20.

Key: 1. Concorde aerodynamic data
2. Basic model
3. Equipped with permeable pods
4. Results
5. ... as a function of...

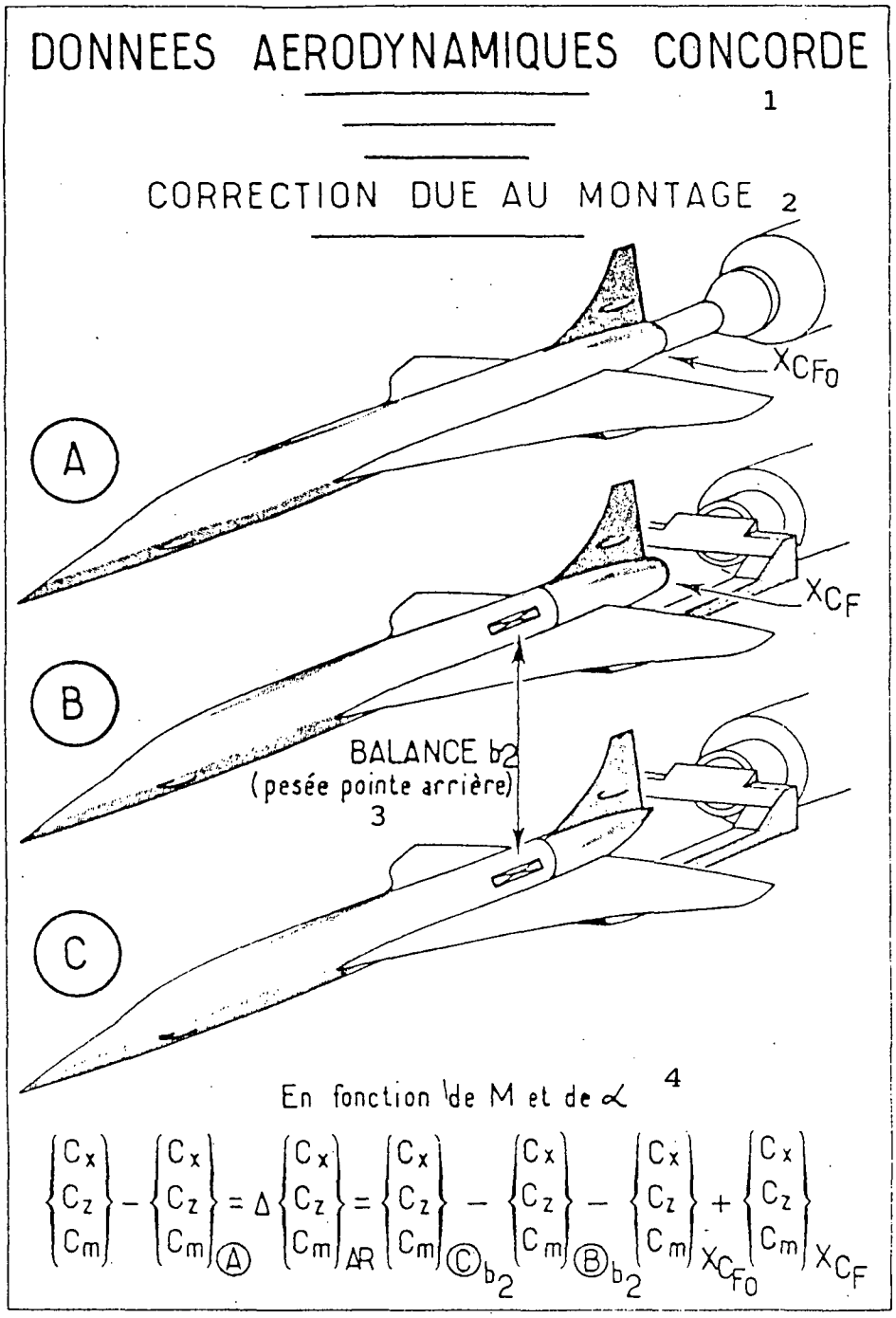

Fig. 21.

Key: 1. Concorde aerodynamic data
2. Correction due to assembly
3. Back end force
4. As a function of M and

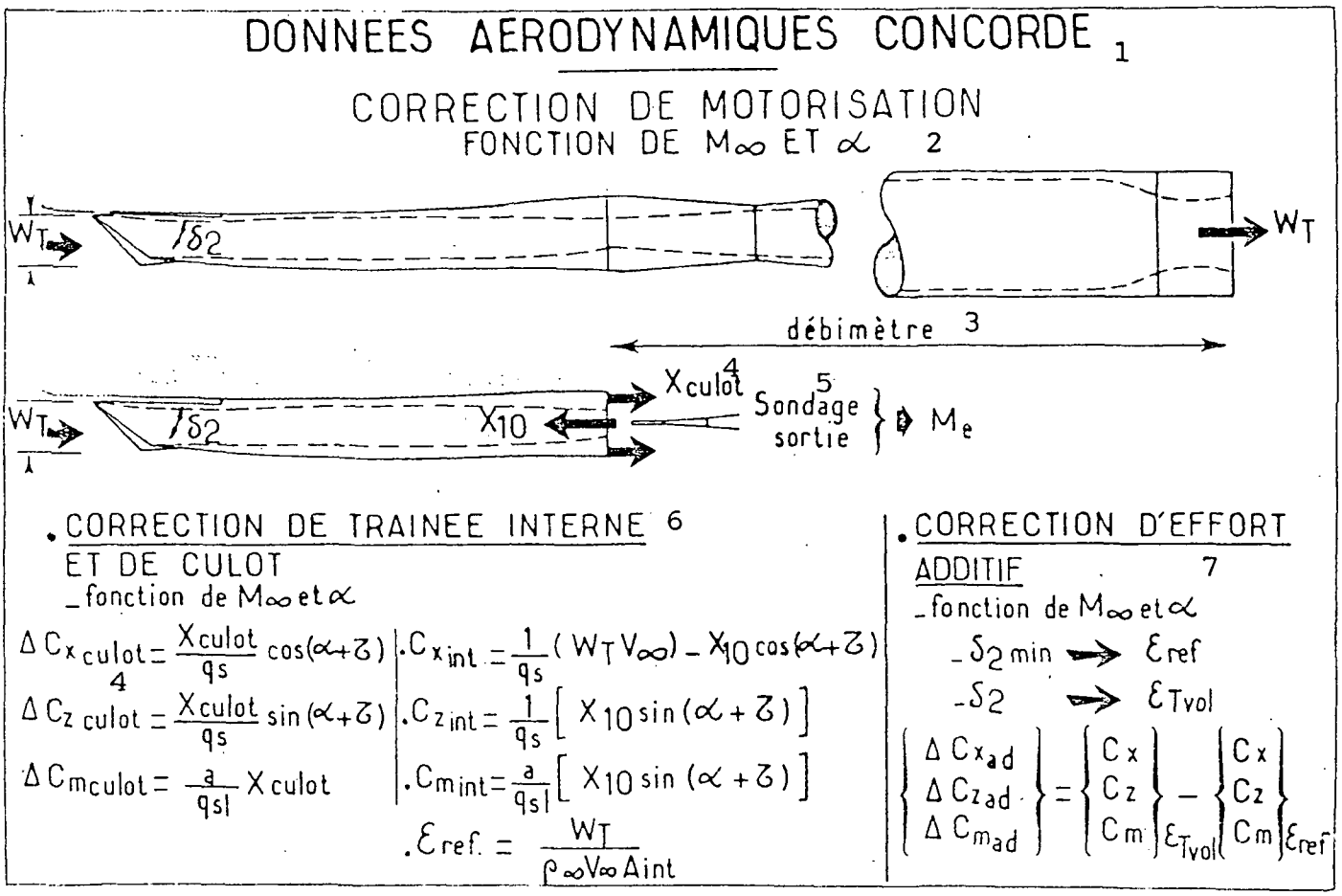

Fig. 22.

Key:
1. Concorde aerodynamic data
2. Motorization correction as a function of M ∞ and α
3. Flowmeter
4. Base
5. Outlet probe
6. Internal drag and base drag correction
7. Additive stress correction

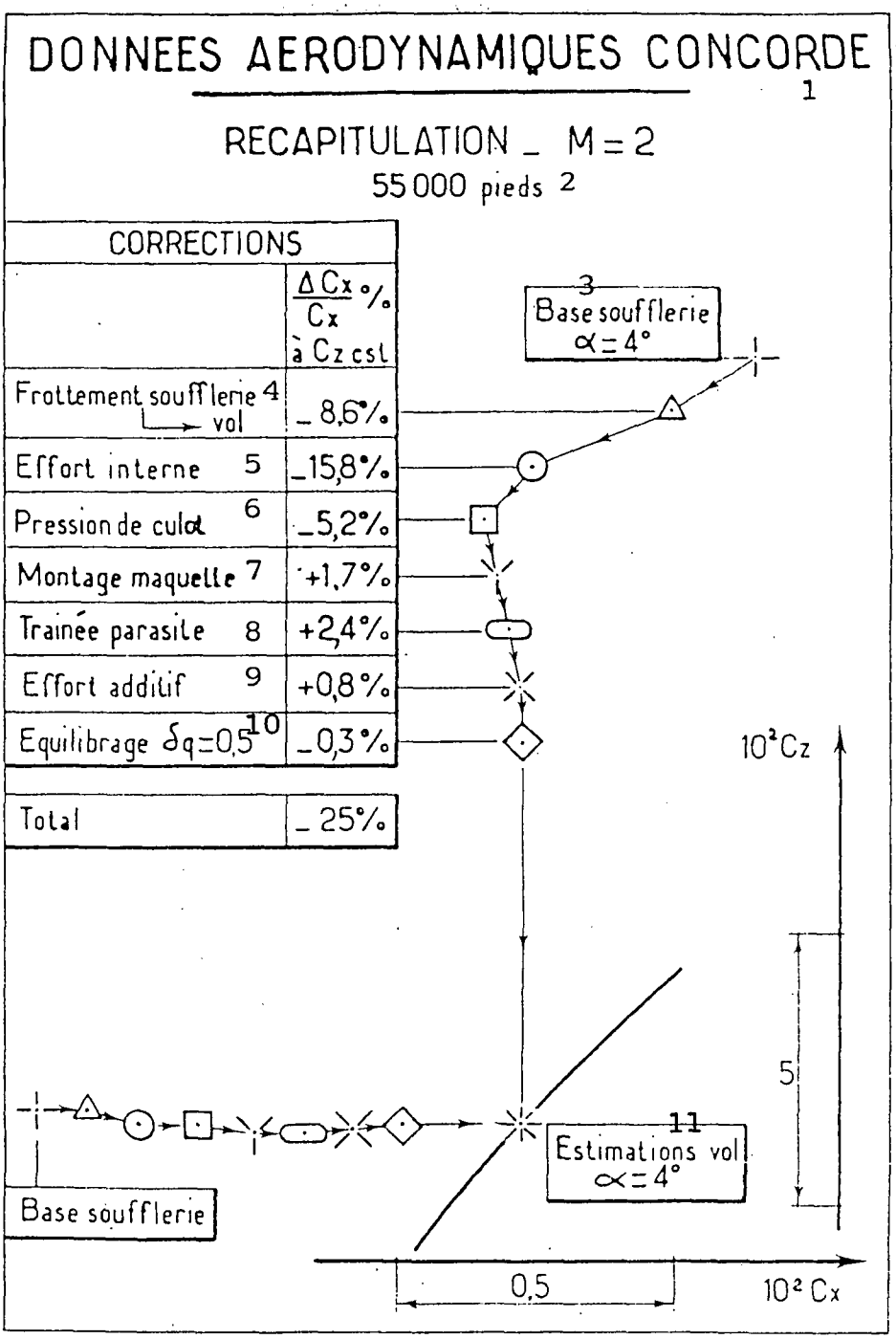

Fig. 23.

Key:
1. Concorde aerodynamic data
2. 55,000 ft.
3. Wind tunnel course
4. Wind tunnel friction - flight
5. Internal stress
6. Base pressure
7. Model assembly
8. Stray drag
9. Additive stress
10. Trim
11. Flight estimations

FLIGHT TEST EQUIPMENT

AIRBUS

Receivers	Anemometric station		Fuselage cowl		Nose probe	Inertial platform		Impulse Motometer	Mass Flowmeter
Parameter	Altitude Pressure	Corrected speed	local incidence	local sideslip	Total temperature	Longitudinal trim	Lateral trim	Fan regime	Fuel flow
symbol	z_p	V_c	α_c	β_c	T_{t_∞}	θ	ϕ	N_1	C
Accuracy	±50ft	±3Kt	±0°3	±0°3	±1,5°K	±0°2	±0°2	0	±100kg/h

Receivers	ZF Westime + gauge	gauge				
parametre	mass	Trim	Steering control			
			elevat.	fixed plane	warp	direction
symbol	m	CG	δ_q	δ_{EH}	δ_p	δ_r
Accuracy	±1000kg	±0,1%	±0,3°			

Fig. 24.

FLIGHT TEST EQUIPMENT

CONCORDE

Receivers	Nose-end Pressure balance		Nose-end cowls		Nose probe	Inertial platform		Accelerometer unit		
paramètre	datum pressure	dynam. pressure	Local incidence	Local sideslip	température total	Longitudinal trim	Lateral trim	accélération longitudinal	accélération latéral	accélération vertical
symbol	p_r	Δp	α_c	β_c	T_{t_∞}	θ	φ	n_{x_1}	n_{y_1}	n_{z_1}
Accuracy	±0,4 mb	±0,4 mb	±0,2°	±0,2°	±0,8° K	±0,2°	±0,2°	± 0,0015 g	±0,003g	±0,0065g

Receivers	Mass flow-meter	Gauge Flow-meter	Impulse moto-meter			
paramètre	Oil flow	mass	regime BP HP	Steering Control Elev.	Warp	direction
symbol	C	m	N_1 et N_2	δq	δp	δr
Accuracy	±0,35%	± 300 kg	≃0	±0,2°		

Fig. 25.

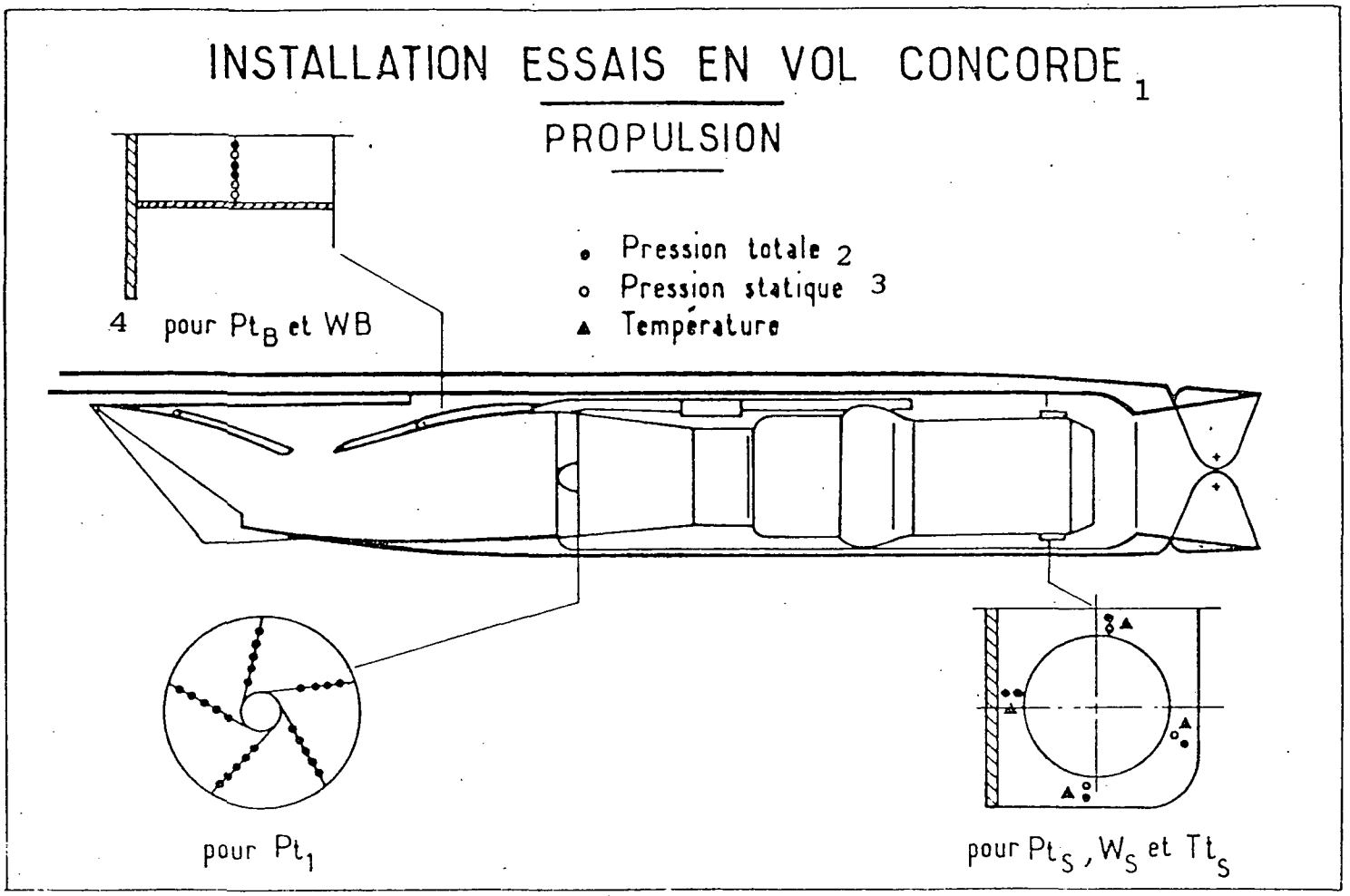

Fig. 26.

Key: 1. Flight test equipment
2. Total pressure
3. Static pressure
4. For...

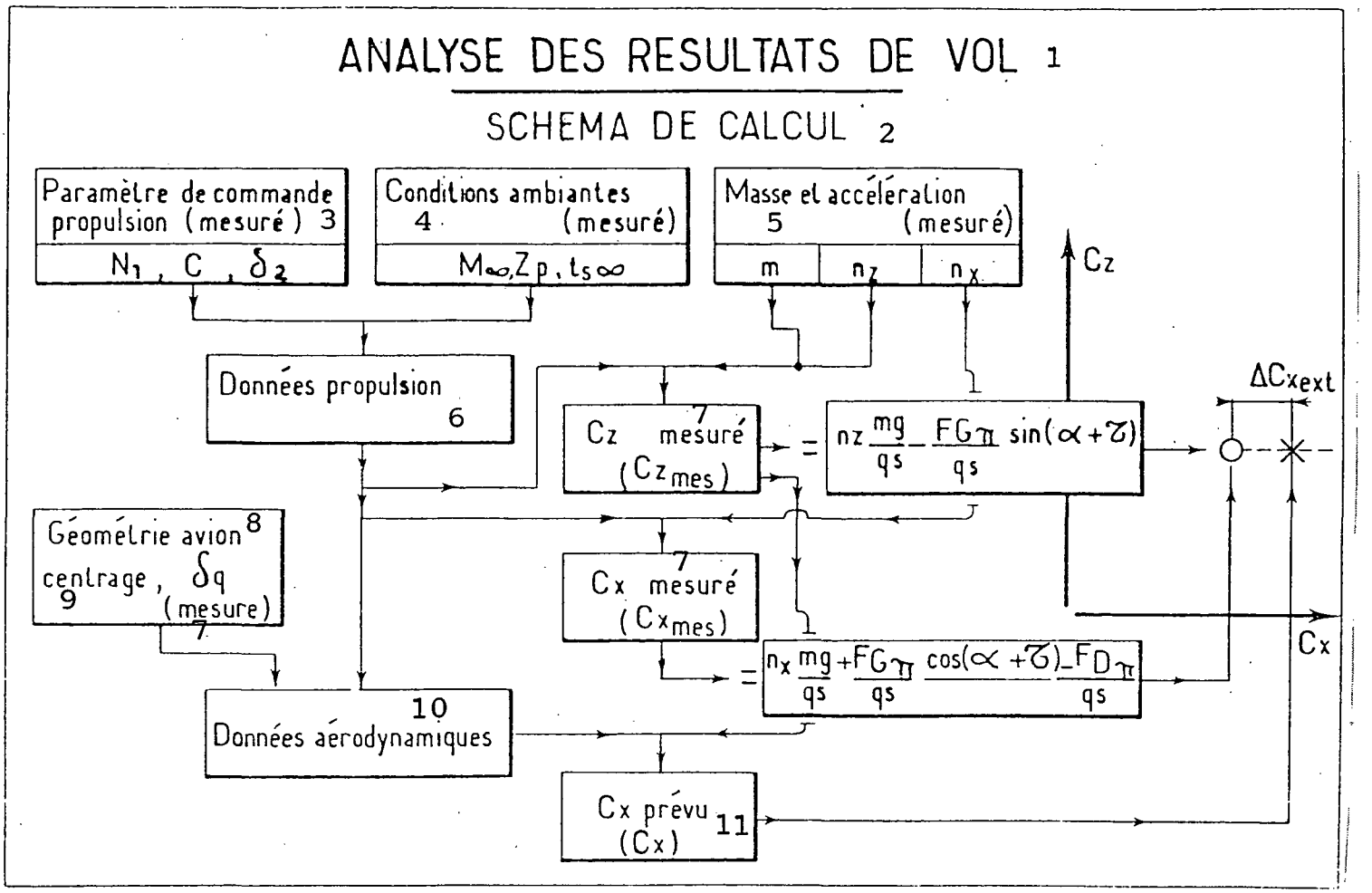

Fig. 27.

Key:
1. Analysis of flight results
2. Outline of calculations
3. Propulsion control parameter (measured)
4. Actual conditions (measured)
5. Mass and acceleration (measured)
6. Propulsion data
7. Measured
8. Plane geometry
9. Trim
10. Aerodynamic data
11. Predicted C_X

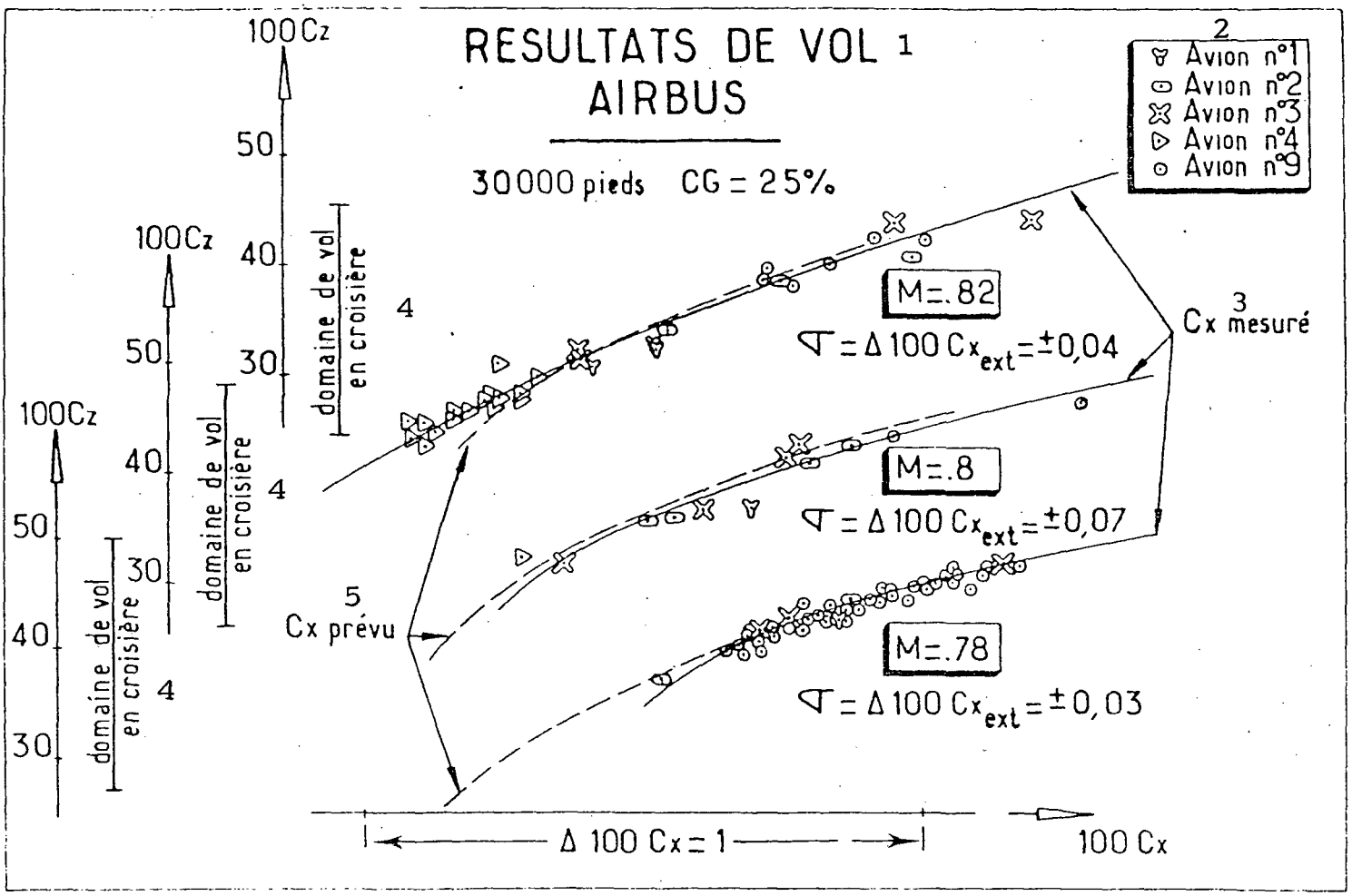

Fig. 28.

Key:
1. Flight results
2. Plane
3. Measured C_X
4. Cruising flight
5. Predicted C_X

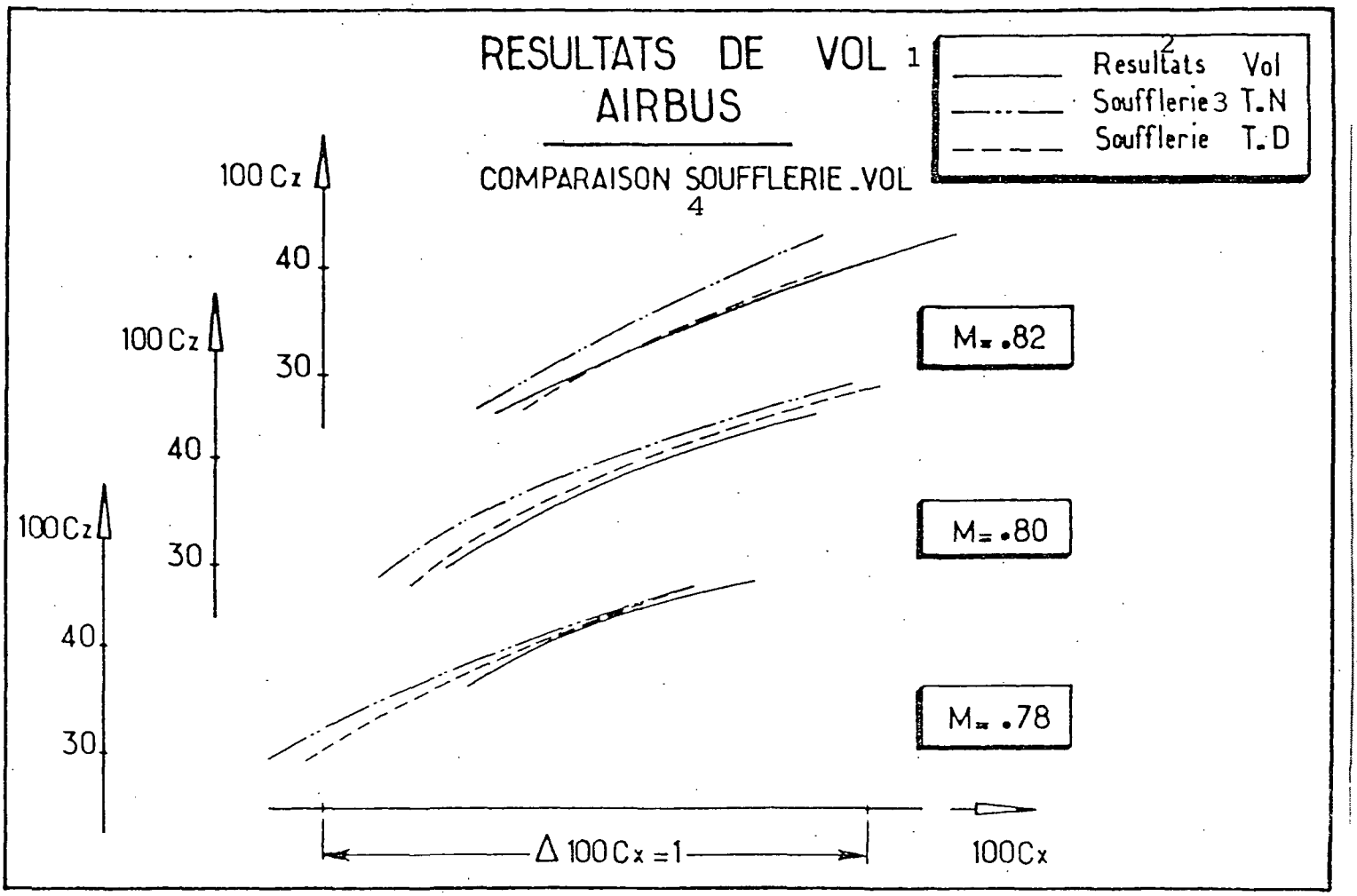

Fig. 29.

Key: 1. Flight results
2. Results
3. Wind tunnel
4. Wind tunnel/flight comparison

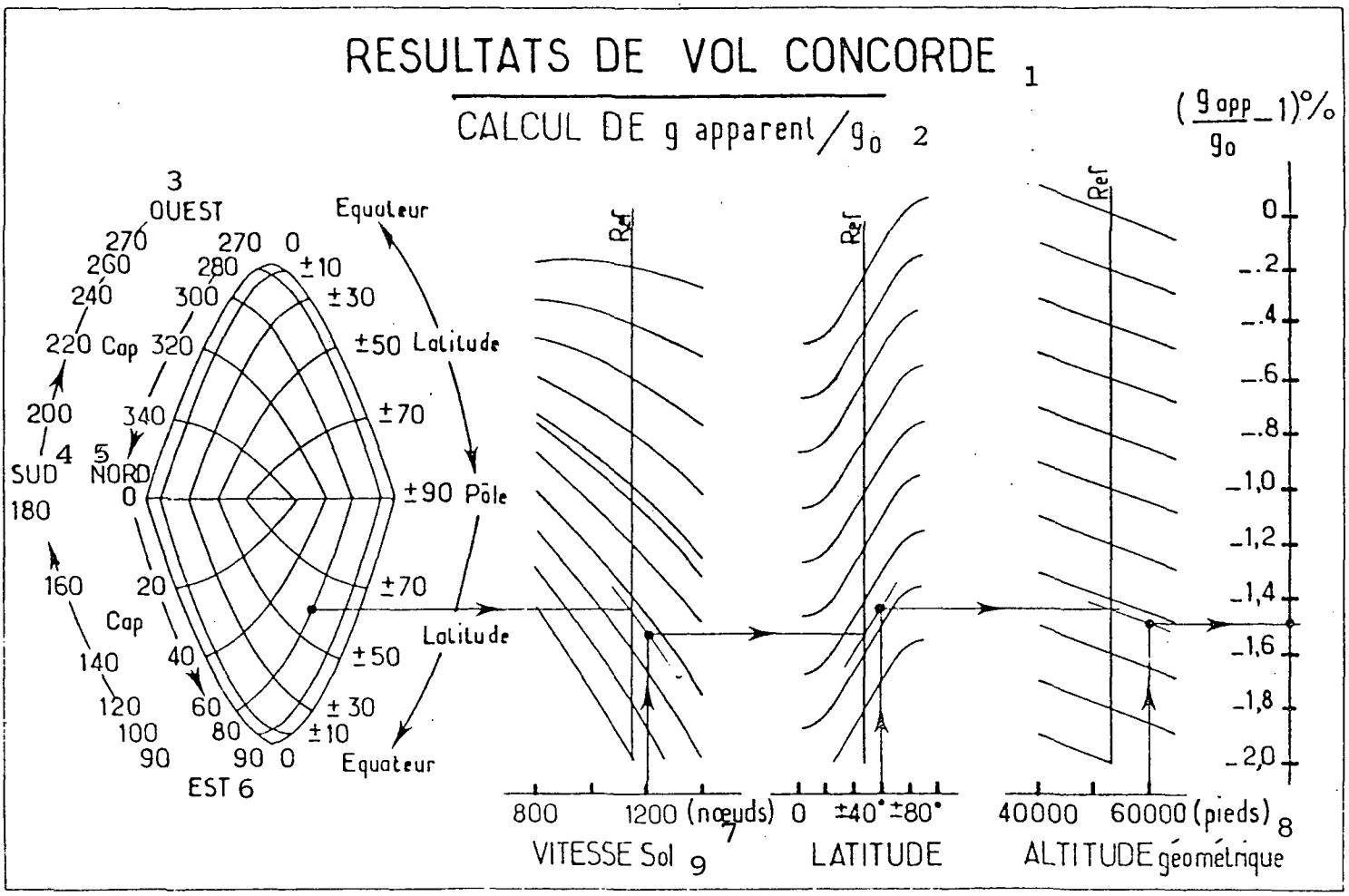

Fig. 30.

Key: 1. Concorde flight results
2. Calculation of apparent g/g_o
3. West
4. South
5. North
6. East
7. Knots
8. Ft.
9. Ground speed

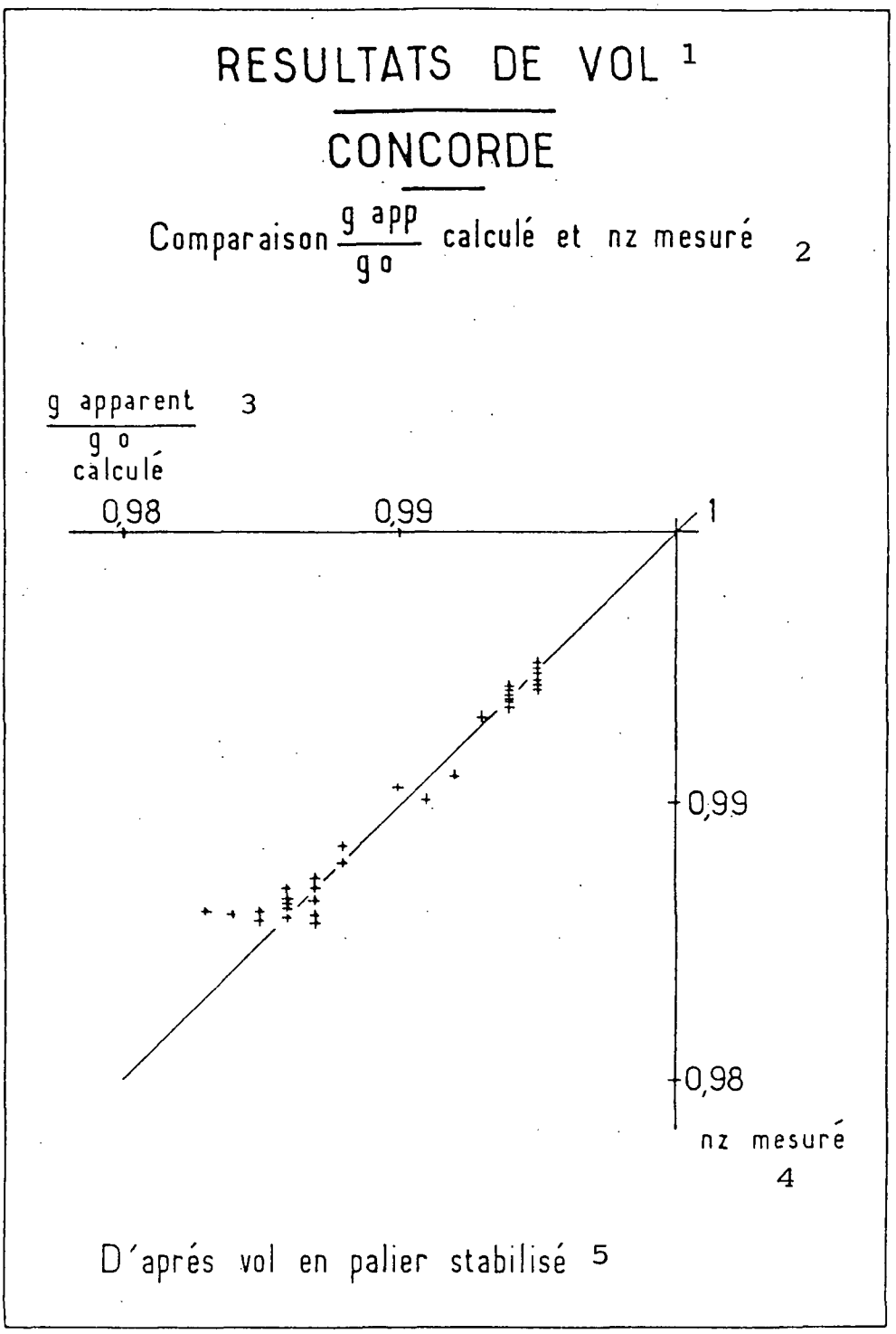

Fig. 31.

Key: 1. Flight results
2. Calculated g_{app}/g_o and measured nz
3. g_{app}/g_o calculated
4. Measured nz
5. Based on stabilized level flight

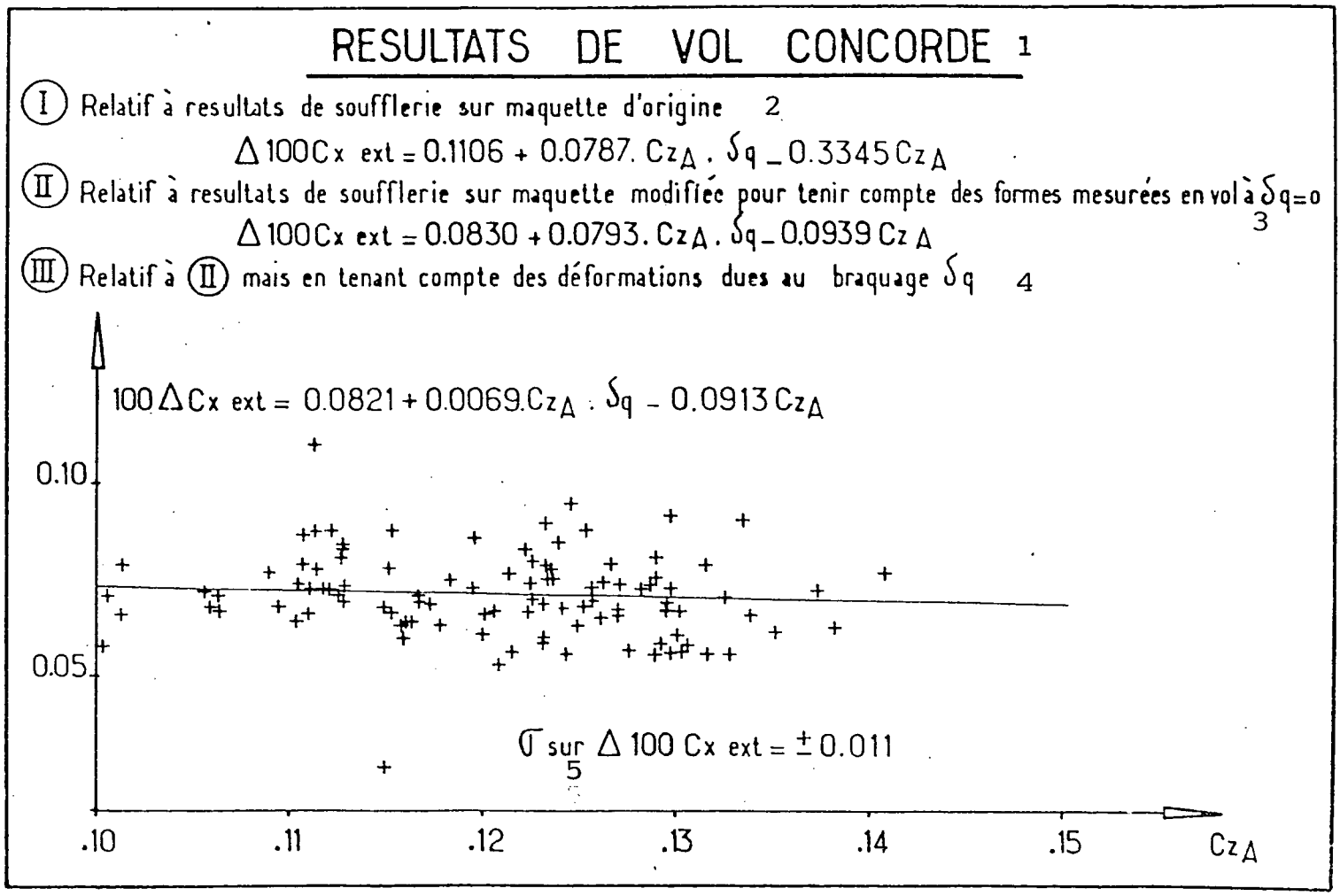

Fig. 32.

Key:
1. Concorde flight results
2. Relative to wind tunnel test results on original model
3. Relative to wind tunnel test results on model modified to take into account shapes measured in flight at $\delta q = 0$
4. Relative to II but taking into account deformations due to angle.
5. On

NOMENCLATURE

M_∞ , V_∞	Mach number and infinite upstream speed
Pt_∞ , Ps_∞	Infinite upstream total and static pressure
ρ_∞	Specific infinite upstream mass
Tt_∞ , $t_{s\infty}$	Infinite upstream total and static temperature
$\Delta\theta$	Standard temperature
q	Infinite upstream dynamic pressure
S	Datum surface
Aint	Air intake datum surface
W_T, ε_T	Air intake flow and total flow coefficient
W_B, ε_B, Pt_B	Flow, flow coefficient and total pressure of Concorde air intake inlet
η_B	Efficiency Pt_B/Pt_∞
W_1, Pt_1, Tt_1	Flow, pressure and total temperature at engine inlet
η_1	Efficiency Pt_1/Pt_∞
W_{Jm}, PtJm, TtJm	Flow, Pressure and total temperature at engine outlet (hot jet)
PtJ_F	Total pressure at fan outlet (Airbus)
W_S, Pt_S, Tt_S	Flow, total pressure and temperature of secondary air at nozzle inlet (Concorde)
Kc	Critical exit correction as afunction of Ttjm for Concorde nozzle
F_{X_A}, C_{X_A}	Drag and drag coefficient of aerodynamic data
F_{Z_A}, C_{Z_A}	Lift and lift coefficient of aerocynamic data
φ	Aerodynamic efficiency: $\varphi = \frac{F_{Z_A}}{F_{X_A}} \equiv \frac{C_{Z_A}}{C_{X_A}}$
α	Angle of aerodynamic incidence
$F_{G\pi}$	Raw thrust of propulsion data
$F_{D\pi}$	Air intake catchment drag
C	Engine oil flow
τ	Raw thrust adjustment on plane's axis
C_{X_B}, C_{Z_B}, C_{m_B}	Drag, lift and pitch momentum coefficients for basic model
ε Ref	Pod flow coefficient for basic model

ΔCX_{AR}, ΔCZ_{AR}, ΔCm_{AR}	Correction due to assembly in wind tunnel
$\Delta C_{X_{int}}$, $\Delta C_{Z_{int}}$, ΔCm_{int}	Correction due to internal drag of pods
$\Delta C_{X_{base}}$, $\Delta C_{Z_{base}}$, ΔCm_{base}	Correction due to pod base (Concorde)
$\Delta C_{X_{jet}}$, $\Delta C_{Z_{jet}}$, ΔCm_{jet}	Correction due to pressure stresses on pods (Airbus)
C_{Xmeas}	Drag coefficient deduced from flight tests
C_X	Drag coefficient predicted at flight Z_{Zmeas}
$\Delta C_{X_{ext}}$	= $(C_{Xmeas} - C_X)$ at C_{Zmeas} in flight
n_x	Acceleration relative to g_o along speed V_∞
n_z	Acceleration relative to g_o perpendicular to speed
g_o	Acceleration of datum weight
m	Mass of plane
δq	Elevator angle
δEH	Horizontal rudder angle (Airbus)
$\delta 2$	Angle of second air-intake pipe (Concorde)
a	Distance of raw thrust axis ($F_{G\pi}$) from gravity center
l	Length of datum cord